First Quarterly Report

STUDY AND APPLICATIONS OF RETRODIRECTIVE AND SELF-ADAPTIVE ELECTROMAGNETIC WAVE CONTROLS TO A MARS PROBE

By: C. A. HACKING   J. A. MARTIN

NASA CR 70704

Prepared for:

NATIONAL AERONAUTICS AND SPACE ADMINISTRATION
TECHNICAL INFORMATION DIVISION
AMES RESEARCH CENTER
MOFFETT FIELD, CALIFORNIA

CONTRACT NAS 2-2933

STANFORD RESEARCH INSTITUTE

MENLO PARK, CALIFORNIA

SRI

November 1965

First Quarterly Report

STUDY AND APPLICATIONS OF RETRODIRECTIVE
AND SELF-ADAPTIVE ELECTROMAGNETIC WAVE CONTROLS
TO A MARS PROBE

Prepared for:

NATIONAL AERONAUTICS AND SPACE ADMINISTRATION
TECHNICAL INFORMATION DIVISION
AMES RESEARCH CENTER
MOFFETT FIELD, CALIFORNIA   CONTRACT NAS 2-2933

By: C. A. HACKING   J. A. MARTIN

SRI Project 5574

Approved: R. C. HONEY, MANAGER
          ELECTROMAGNETIC TECHNIQUES LABORATORY

          D. R. SCHEUCH, EXECUTIVE DIRECTOR
          ELECTRONICS AND RADIO SCIENCES

Copy No. ....

CONTENTS

ILLUSTRATIONS

TABLES

I INTRODUCTION

This first quarterly report will incorporate the third monthly report as well as include some of the information reported in the first two montly reports.

At the end of the first quarter approximately 8.5 percent of the total contract funds have been expended, but the rate of expenditure has increased to a present value of about 7 percent per month. This rate will be increased still further during the next period, and it is anticipated that nearly 50 percent of the funds will have been expended by the end of the second quarter.

The project has been divided into three tasks, which are listed below together with the task leaders and laboratories with which they are associated.

TASK 1   Antenna Concepts: System and analysis aspects of antenna configurations. The task leader (and also project leader) is C. A. Hacking of the Electromagnetic Techniques Laboratory.

TASK 2   Environmental Conditions: Specific environmental conditions and their effect on system and component configurations. The task leader is J. A. Martin of the Electromagnetic Sciences Laboratory.

TASK 3   Phase-Lock Loops and Adaptive Circuitry: Circuitry behind the antenna elements. The task leader is C. H. Dawson of the Radio Systems Laboratory.

Apart from the literature searches, most of the work done so far on the project has been concerned with Tasks 1 and 2. During the third month of the quarter, significant progress was made on the study of two possible cylindrical antenna configurations. At present, consideration has been restricted to spin-stabilized vehicles in which the spin axis is nearly perpendicular to the desired direction of transmission of information.

1

The direction of Task 2, the environment study, has been toward summation of characteristics and consideration of the effects of environment upon retrodirective antenna operation. Both the environment of an orbiting or fly-by bus and that of a re-entry capsule are being considered. A literature search has been conducted.

At present there is no unique definition of an adaptive antenna, although proposed definitions for adaptive, retrodirective, self-steering, and other types of antenna have been put forward in meetings of the IEEE's Committee 2, of which one of the SRI staff is a member. It therefore seems necessary for us to make our own definitions of some of the commonly used terms in order to avoid confusion. It is hoped that these definitions will not vary appreciably from those eventually adopted by the IEEE. These definitions are as follows:

Adaptive antenna - A generic term including all antennas having a receiving and/or transmitting beam that is controlled by the direction of one or more incoming signals. Such an antenna may be active or passive. (One simple form of an adaptive antenna is the well-known corner reflector.)

Retrodirective antenna - An antenna which radiates its major lobe back in the direction from which a pilot signal is received. (This is the definition proposed by S. P. Morgan of Bell Telephone Laboratories and apparently accepted by Committee 2 of the IEEE.)

Self-steering antenna - A special type of adaptive antenna array which adjusts phases of element signals to allow in-phase addition, thereby extracting maximum power from the incident signal, even if it is in the radiating near field of the aperture (in which case, it is called self-focussing). A self-steering antenna may be used for receiving only, or it may transmit as well. (This definition has been suggested by R. C. Hansen but has not yet been adopted as a standard.)

II PERFORMANCE DURING THE FIRST QUARTER

A. TASK I - ANTENNA CONCEPTS

1. Basic Antenna Configurations

Computer studies of two novel types of adaptive antennas with
circular symmetry have been started. So far the studies have been con-
fined to the retrodirective class of antennas, but the study machinery
could readily be adapted to self-steering antennas having the same gen-
eral antenna configuration. The basic aim of the present study is to
determine antenna parameters which provide the maximum effective radiated
power (ERP) in the desired direction for any given fixed amount of elec-
trical power available in the space craft for transmission purposes.

Each of the two antennas consists of a cylindrical geodesic
lens with one end connected to a radiating structure and the other end
connected to receiving and/or transmitting elements. The only difference
between the two antennas being investigated is that on one of them a
biconical horn is used as the radiator, while on the more complex version,
a cylindrical array of line source radiators is used as the free-space
radiator. The latter antenna has much greater potential for decreasing
the beamwidth in the axial plane, but the present study is only con-
cerned with antenna patterns in the azimuthal plane. For the present,
therefore, the term "azimuthal gain" will be used and will represent the
gain of the particular antenna with respect to an antenna having similar
beamwidths in the axial plane but having an omnidirectional azimuthal
antenna pattern. Thus, the axial-plane aperture and antenna beamwidth
will not be considered in this report.

Figure 1 shows a general configuration of the cylindrical-
geodesic-lens, biconical-horn adaptive antenna as well as the principal
dimensions used in the computater study. Also shown are the N principal
rays from the N radiating structures, which, it is assumed, make up the
collimated RF beam. Each of these rays represents the shortest distance
between the particular elemental radiator and the "distant observation
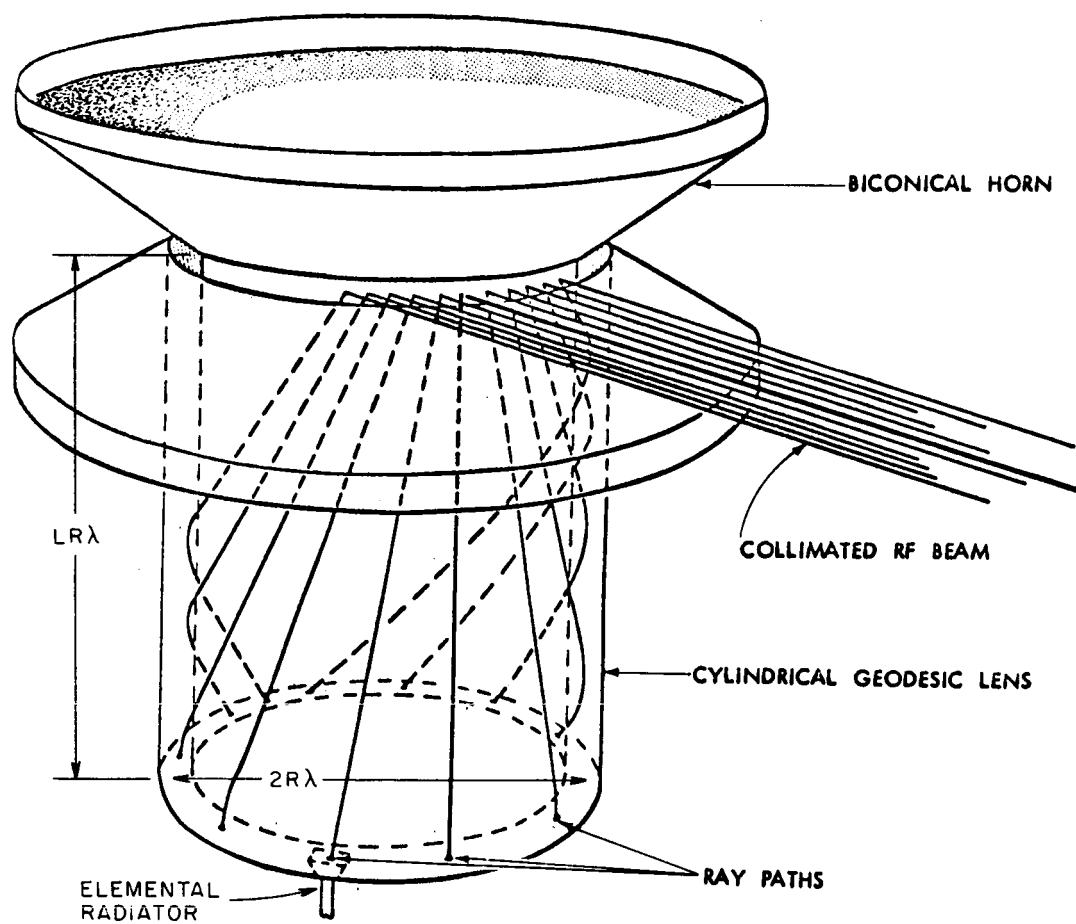
Labels within figure:
BICONICAL HORN
COLLIMATED RF BEAM
CYLINDRICAL GEODESIC LENS
RAY PATHS
ELEMENTAL RADIATOR
LRλ
2Rλ
TA-5574-1

FIG. 1 CYLINDRICAL-GEODESIC-LENS BICONICAL-HORN ADAPTIVE ANTENNA

point". Of course, this figure is an over simplification, since radiation occurs in many directions from each of the elemental antennas and is eventually radiated by the biconical horn in all azimuthal directions, but this radiation does not, in general, add in phase except in the direction of the main beam. In the present study it is assumed that the values of L and R and the radiation pattern of each elemental radiator within the geodesic lens [denoted by $G(\alpha)$] are such that only two rays from each elemental radiator contribute significantly to the final antenna radiation pattern for any particular azimuthal direction. One of these rays travels around the cylindrical lens in one direction, while the other travels in the opposite direction. The inaccuracies introduced by this assumption or simplification do not appear to be substantial, particularly when compared with the other assumptions and simplifications (such as the use of ray optics) employed in this study.

Figure 2, in which the cylindrical lens portion of the antenna is shown in its "developed" form, indicates the geometry used for the discrete-radiator cylindrical-geodesic-lens antenna. Also shown is a grossly oversimplified figure of the wave fronts and ray-optic rays within the cylindrical lens region. The computations of the radiation pattern from an antenna of this type are considerably more lengthy than those for the biconical-horn antenna. Indeed, the computation of a single radiation pattern for an antenna of many elements is likely to tax the storage capacity of even the largest digital computer. Radiation patterns of a typical antenna using discrete line-source radiators have not yet been obtained, but a computer program which can compute the pattern with reasonably economy is being developed.

2.   Theory of the Analysis Procedure

Some of the analysis procedure is common to both of the above types of antenna, but only the specific procedure used for considering the biconical-horn antenna is discussed below. In addition to the assumptions mentioned above, two other important assumptions have been made for this analysis: (1) that the mutual couplings between the elemental radiators at the bottom of the geodesic lens are negligible,

TYPICAL RADIATOR ELEMENT

CYLINDRICAL LENS

EACH TOP
WAVE GUIDE
CONNECTED TO
A HORIZONTALLY
DIRECTED RADIATOR

ONLY 25 TO 35% OF RADIATORS ARE
ILLUMINATED AT ANY INSTANT

WAVE FRONTS

RAYS

0   180   360

CYLINDRICAL LENS "ROLLED OUT" INTO PLANE OF PAPER
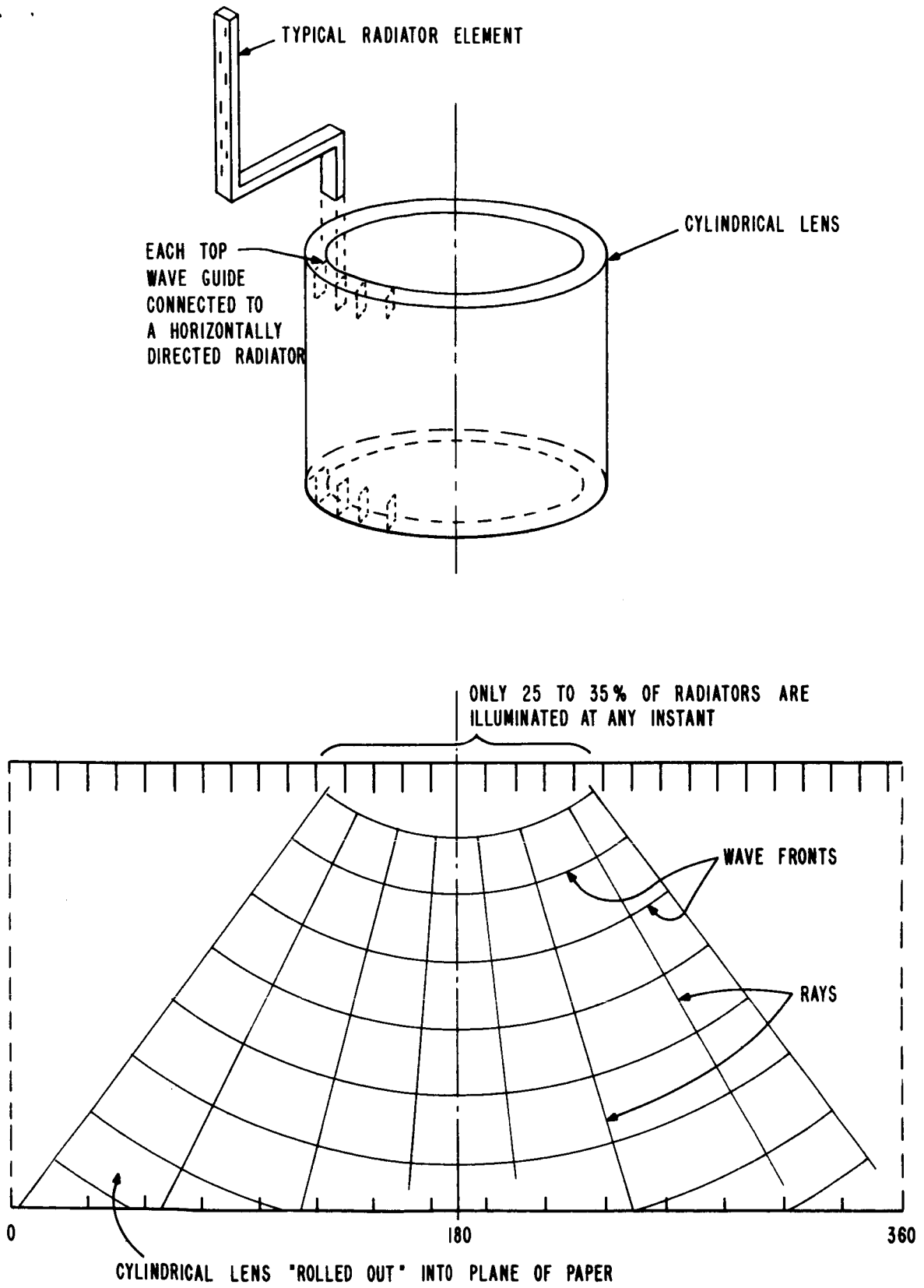
TA-5574-2

FIG. 2 A CYLINDRICAL-GEODESIC-LENS MULTIPLE-LINE-SOURCE ANTENNA

6

and (2) that the discontinuity between the biconical horn and the
coaxial cylinders presents a negligble mismatch to all the significant
rays considered in the analysis. Neither of these assumptions is con-
sidered to be a serious limitation of the analysis.

The procedure adopted in this analysis was as follows: The
radiation pattern, described in both amplitude and phase by $B(\gamma)e^{j\psi(\gamma)}$,
was first computed for the biconical antenna with the assumption that
just a single elemental radiator at the bottom of the geodesic lens was
excited. The ray geometry associated with such an element, and a parti-
cular azimuthal direction γ, is shown in Fig. 3. A portion of the
modulus of such a typical amplitude function or pattern is reproduced
in Fig. 4 for azimuthal angles γ from 0 to 180 degrees. The elemental
radiator is situated at $\gamma = 0$, and the pattern is, of course, symmetri-
cal; its derivation is considered in more detail below. It will be
noted that this pattern is much more nearly omnidirectional than the
radiation pattern of the element itself within the cylindrical geodesic
lens, which is also plotted in Fig. 4 as a function of α, using the
same angle scale. Indeed, the lens may be said to transform the ori-
ginal relatively narrow beam into an approximately omnidirectional pat-
tern, albeit with some severe interference ripples. This pattern will
be referred to as the "single-element pseudo-omni" pattern.

By reciprocity, this pattern can be treated as either the
transmitting or receiving pattern associated with one element. For the
present computations, the further assumption is made that the trans-
mitting antenna is essentially identical (in wavelength) to the re-
ceiving antenna. If the same antenna is used for both transmitting and
receiving, then the receiving and transmitting frequencies must be very
close together.[1] If different antennas are used, one should be an exact
scale model of the other, the scale factor being the ratio of the re-
spective wavelengths. This latter arrangement allows for any separa-
tion between the two frequencies.

---

*
Superscript numbers refer to the References at the end of this
report.
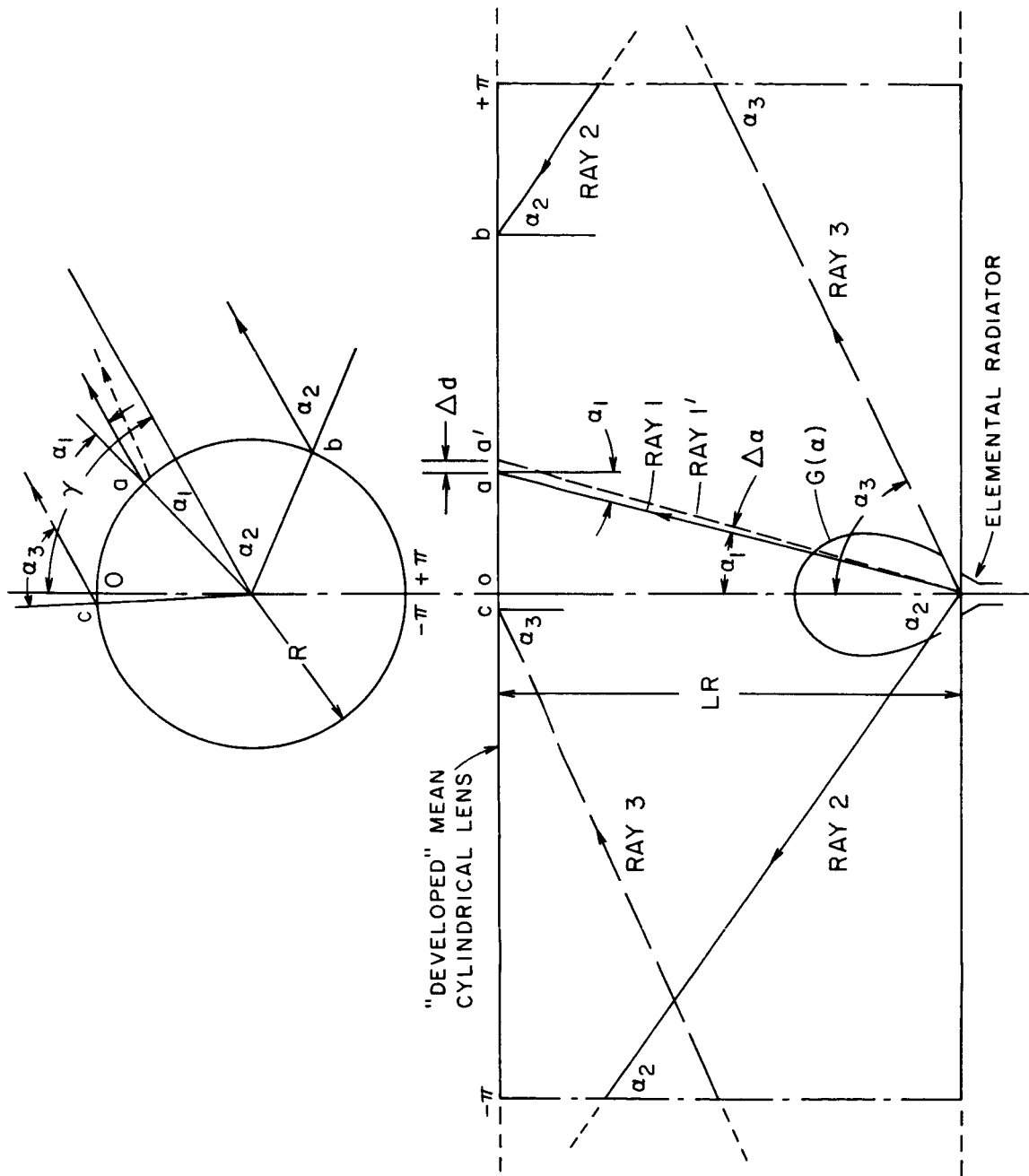
FIG. 3 RAY GEOMETRY ASSOCIATED WITH A SINGLE RADIATOR AND SINGLE AZIMUTH ANGLE

TA-5574-3

8
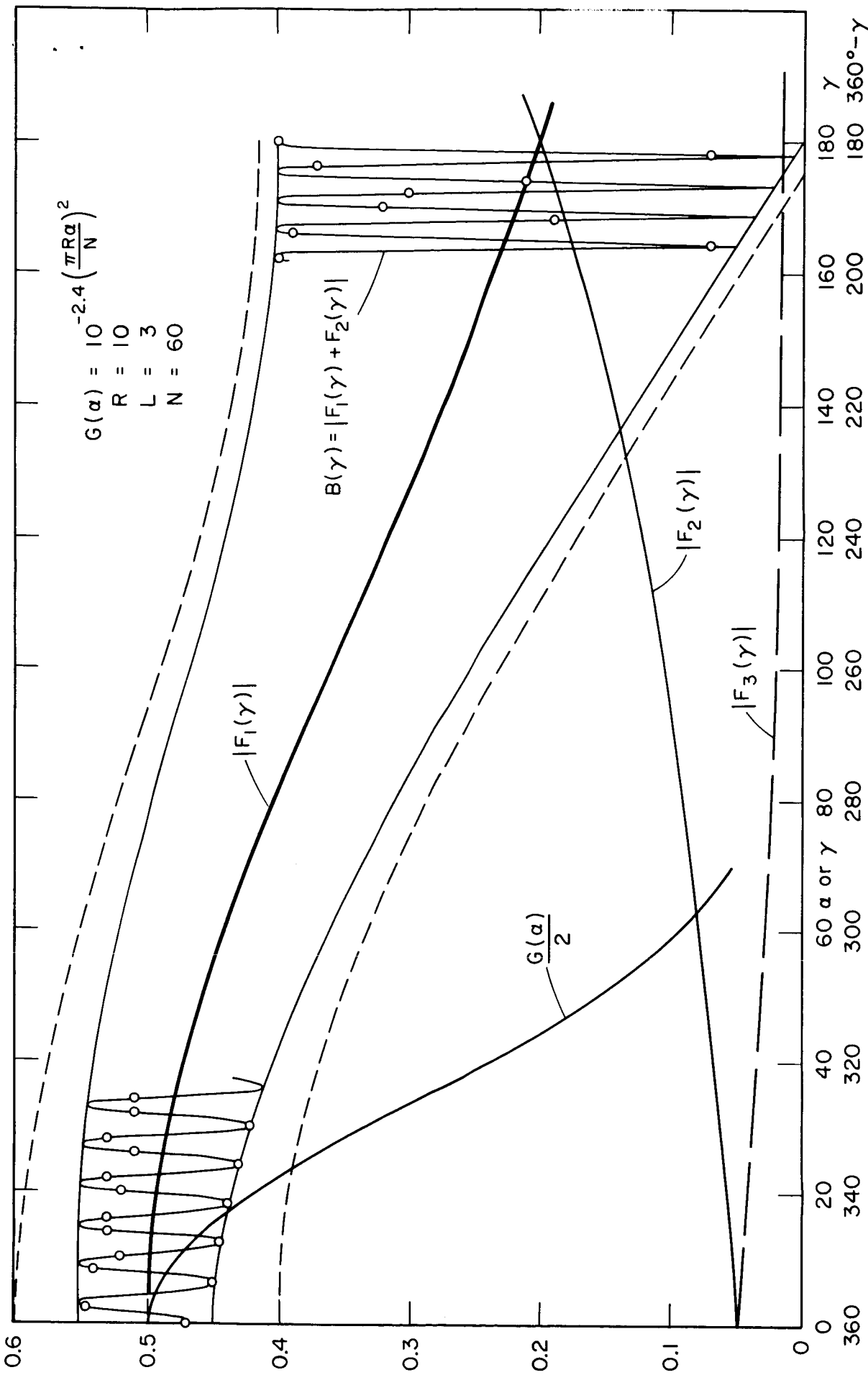
FIG. 4   RADIATION COMPONENTS FROM A SINGLE ELEMENTAL RADIATOR

$$G(\alpha) = 10^{-2.4 \left(\frac{\pi R \alpha}{N}\right)^2}$$
$$R = 10$$
$$L = 3$$
$$N = 60$$

$B(\gamma) = |F_1(\gamma) + F_2(\gamma)|$

$|F_1(\gamma)|$

$|F_2(\gamma)|$

$|F_3(\gamma)|$

$\dfrac{G(\alpha)}{2}$

$60 \ \alpha \text{ or } \gamma$

γ

$360° - \gamma$

TA-5574-4

9

In the receiving mode, the ordinate of the pattern represents the signal received by the particular element as a function of the azimuthal angle γ of the whole structure when the structure is illuminated by unit radiation from that particular azimuthal direction. The technique now being considered to make the antenna structure retrodirective is to provide electronic circuitry, sometimes called a conjugate network, to operate on the incoming signal at each element in such a way that the element then reradiates a signal which has a relative phase angle of sign opposite to that of the incoming signal. In addition, the electronic circuitry will amplify and thus determine the amplitude of the reradiated signal.

The reradiated amplitude could theoretically be made to have any desired relationship to the incoming amplitude, but for the present only two reradiated amplitude functions are being considered in the computer program. These are referred to as "modes of operation," or simply "modes". In Mode 1 all elements radiate with equal amplitude, while in Mode 2 they reradiate an amplitude directly proportional to the received amplitude at that element. In practice, this can be implemented as follows: In Mode 1, the final elemental amplifiers are each driven into saturation and thus deliver maximum RF power regardless of the incoming signal strength. In Mode 2, linear amplifiers are used to amplify the incoming signals in such a way that no output amplifier is ever saturated. In theory, a higher effective reradiated power is to be expected if the available RF transmitter power is distributed to the various elements of an array in proportion to the gains of each of the elements measured in the particular direction in which it is desired to optimize effective radiated power. Mode 2 operation would distribute the power in this optimum manner, but at present it does not appear possible to obtain as high a conversion efficiency from DC to RF for Mode 2 as for Mode 1.

In order to compute the reradiated antenna pattern, the principle of superposition is used to add the amplitudes (vectorially) of the patterns from each of the N elemental radiators. The relative phase of each of these elemental radiators is automatically adjusted by the

10

conjugate network to put in phase the contribution from each element, when observed from the direction of the incoming (pilot) signal. The pattern radiated from the biconical horn when a single element is illuminated is derived as described below.

With reference to Figs. 1 and 3, the following parameters are defined:

$R\lambda$ is the mean radius of the cylindrical geodesic lens and also the throat diameter of the biconical horn.

$LR\lambda$ is the length of the cylindrical lens.

$G(\alpha)$ is the radiation pattern of each elemental radiator within the geodesic lens.

α is the angle measured from the axis of each elemental radiator within the cylindrical geodesic lens and is therefore the angle that a particular ray makes with the direction of the main lobe of the elemental antenna. It is also the angle of incidence and reflection at the right-angle junction between the cylindrical and radial (biconical) lines.

γ is the azimuthal angle.

From Fig. 3, it is seen that

$$\tan \alpha = \frac{R\ (2\pi n + \gamma - \alpha)}{LR} \qquad \text{where } \pm\ n = 0,\ 1,\ 2\ldots$$

which leads to the following very useful, but trancendental, parametric equations:

$$\alpha_1 + L \tan \alpha_1 = \gamma \qquad\qquad \text{for ray 1}$$

$$\alpha_2 + L \tan \alpha_2 = 2\pi - \gamma \qquad\qquad \text{for ray 2}$$

$$\alpha_3 + L \tan \alpha_3 = 2\pi + \gamma \qquad\qquad \text{for ray 3} \quad \text{etc.}$$

11

It can also be seen from the geometry that the higher-order rays contribute progressively lesser amounts of energy in the direction γ, because the gain function $G(\alpha)$ of the elemental antenna decreases and the space taper increases with α.

In order to determine the space taper for the biconical structure, consider the power radiated from an elemental radiator between the angles α and $\alpha + \Delta\alpha$.* The power density of the radiation into this angle $\Delta\alpha$ can be defined as

$$G(\alpha)^2 \text{ watts/unit angle} \qquad \text{is } \Delta\alpha \text{ is small.}$$

The total power radiated into $\Delta\alpha$ is then $G(\alpha)^2\Delta\alpha$. Since we assume there is a perfect match at the transition, this same power is radiated from the biconical antenna, after reflection from the junction between the cylindrical and biconical lines, into an angle $\Delta\epsilon$ (defined in Fig. 5), resulting in a power density

$$G(\alpha)^2 \frac{\Delta\alpha}{\Delta\epsilon} \qquad .$$

Now, at some distant observation point, point p (see Fig. 5) is indistinguishable from point q, except for a phase term, so that $\Delta\epsilon$ is equivalent to a small azimuthal angle $\Delta\gamma$ of equal value. Hence,

$$\left| F(\gamma) \right| = G(\alpha) \quad . \quad \sqrt{\frac{\Delta\alpha}{\Delta\epsilon}} \qquad ,$$

where $F(\gamma)$ is the complex amplitude function of the biconical horn (excluding the effects of multipath interference).

---

*It will be assumed that the space taper in the azimuthal direction for radiation from the biconical horn is independent of the space taper in the axial (elevation) plane. This is a common and usually satisfactory simplification in the computation of antenna patterns. The effect of axial space taper will therefore be neglected at present, since it applies equally to the radiation patterns to be computed and to the patterns of the hypothetical omni-azimuthal antenna, which, as has been mentioned above, is being used as the reference antenna.
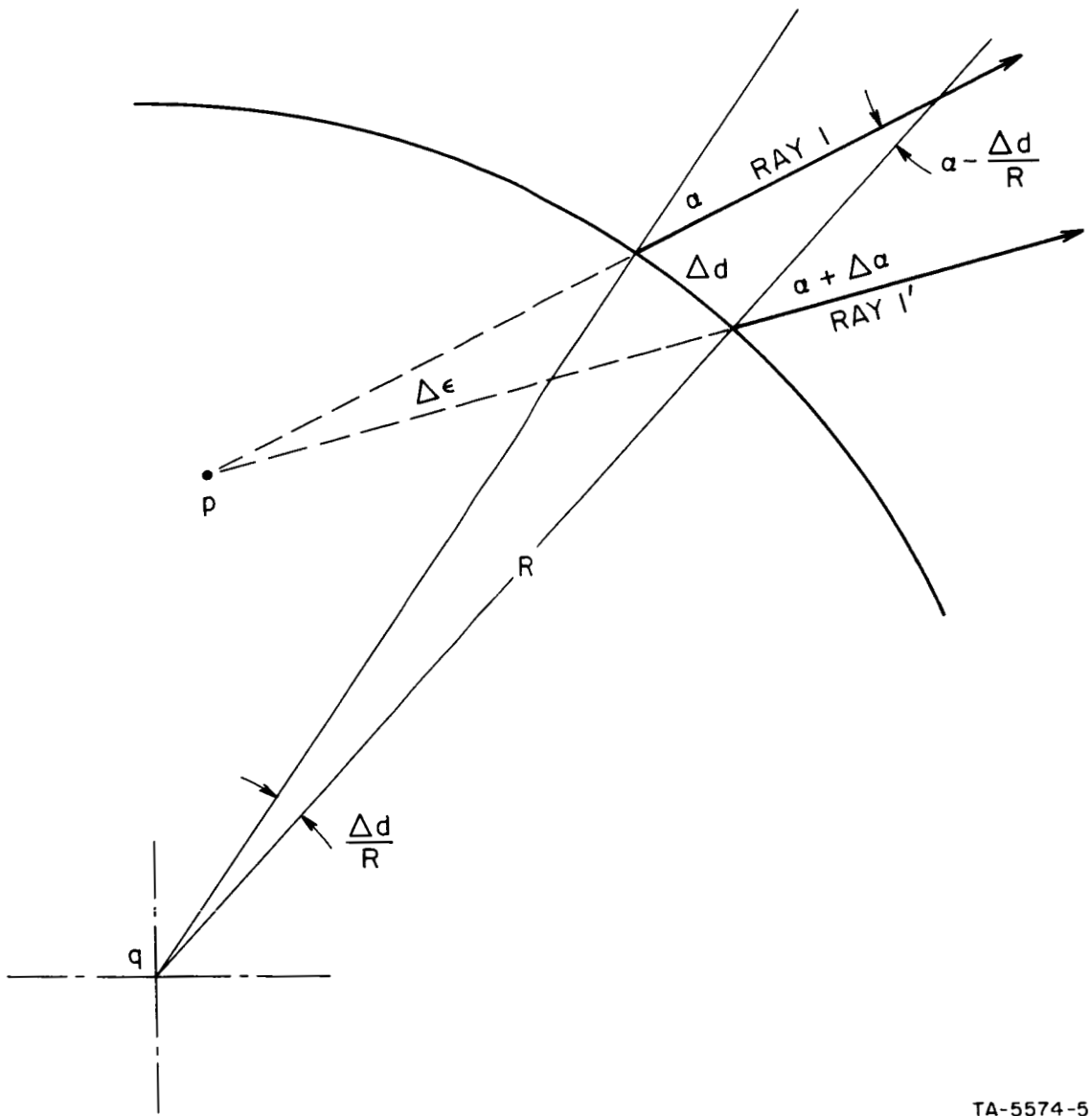
TA-5574-5

FIG. 5   ENLARGEMENT OF PORTION OF FIG. 3 SHOWING THE APPARENT SOURCE
OF RADIATION

Refering to Fig. 3,

$$\Delta d = LR \left[\tan (\alpha + \Delta\alpha) - \tan \alpha \right]$$

$$\frac{\Delta d}{R} = L \frac{\tan \alpha + \tan \Delta\alpha - \tan \alpha + \tan \Delta\alpha \, \tan^2\alpha}{1 - \tan \Delta\alpha \, \tan \alpha}$$

$$= L \, \Delta\alpha \frac{1 + \tan^2 \alpha}{1 - \Delta\alpha \, \tan \alpha} \qquad \text{since } \tan \Delta\alpha = \Delta\alpha \text{ if } \Delta\alpha \text{ is small}$$

Refering to Fig. 5,

$$\Delta\epsilon = (\alpha + \Delta\alpha) - (\alpha - \frac{\Delta d}{R})$$

$$= \Delta\alpha \left(1 + L \frac{\text{Sec}^2\alpha}{1 - \Delta\alpha \, \tan \alpha} \right)$$

$$\text{and } \lim_{\Delta\alpha \to 0} \quad \Delta\epsilon = \Delta\alpha \, (1 + L \, \text{Sec}^2 \alpha) \qquad \text{except where } \alpha \to \pm \frac{\pi}{2}$$

Hence,

$$\left| F(\gamma) \right| = G(\alpha) \, (1 + L \, \text{Sec}^2\alpha)^{-1/2} \qquad .$$

To determine the relative phase of the radiation again associated with a single elemental radiator and observed at points at a large but constant distance D from the center of the biconical structure, consider at length of each ray, or geodesic, as a function of γ, or more conveniently as a function of α:

The length within the lens is L R λ Sec α.

The length outside the lens is D - R λ Cos α.

The relative length is then $R\lambda \left(\dfrac{L}{\text{Cos } \alpha} - \text{Cos } \alpha \right)$, and the

relative phase difference is $2\pi \, R \left(\dfrac{L}{\text{Cos } \alpha} - \text{Cos } \alpha \right)$.

14

Hence,

$$F(\gamma) = \frac{G(d)}{\sqrt{1 + L \, \text{Sec}^2 \, \alpha}} \, \exp\left[j \, 2\pi R \left(\frac{L}{\text{Cos} \, \alpha} - \text{Cos} \, \alpha \right) \right] \quad .$$

As can be seen from Fig. 3, there is more than one ray, or geodesic, (i.e., line of minimum electrical length) joining the elemental radiator with any distant observation point, depending on which way the ray turns around the cylinder and how many turns it mades within the cylindrical portion of the antenna. These several rays will interfere with each other to produce ripples in both amplitude and phase as a function of azimuthal angle γ. The amplitudes of the first-, second-, and third-order rays are plotted in Fig. 4 for some typical antenna parameters.

It can be seen that the third-order ray is everywhere less than 10 percent (> 20 dB down) of the first-order or principal ray, therefore for the purposes of the computation it was neglected. This simplification can be justified on the grounds that this ray optics technique is not exact enough to give any more than an indication of the main beam, the gain, and the general maximum side-lobe levels. In addition, the very principle of operation of the retrodirective antenna array employing conjugate networks tends to compensate automatically for such perturbations as the effects of mutual coupling, and in this case, higher-order rays.

Because the length of the first-order ray increases with γ, while the second-order ray decreases, the addition of $F_1(\gamma)$ and $F_2(\gamma)$ produces an interference pattern whose amplitude varies between

$$\left| F_1(\gamma) \right| \pm \left| F_2(\gamma) \right| \quad .$$

These limits are shown in Fig. 4 as well as portions of

$$B(\gamma) = \left| F_1(\gamma) + F_2(\gamma) \right| \quad ,$$

15

based on points computed every two degrees. If $F_3(\gamma)$ had also been taken into account, $B(\gamma)$ would have varied between the two dashed limits shown in Fig. 4, but the curve of $B(\alpha)$ would be somewhat more complex than the actual curve shown.

The elemental antenna amplitude function $G(\alpha)$ used in these initial computations was somewhat arbitrarily chosen to give the antenna a 3-dB beamwidth of 1 radian per $\dfrac{\text{aperture}}{\text{wavelength}}$ and a commonly used parabolic-logarithimic beam shape; i.e., the beamwidth relationship over the angles of interest is given by

$$\frac{dB_1}{dB_2} = \left(\frac{\alpha_1}{\alpha_2}\right)^2 \quad .$$

It has been further assumed that the bottom of the cylindrical lens is completely filled with contiguous elemental antennas. Thus, the size of each aperture is $\dfrac{2\pi R}{N}$ wavelengths. This leads to an elemental emplitude function given by

$$G(\alpha) = 10^{-2.4 \left(\frac{\pi R \alpha}{N}\right)^2} \quad ,$$

which has been used for all the computations to date.

a. Computation of the Reradiation Pattern

Once the radiation pattern of the biconical horn due to a single elemental antenna, given by

$$B(\gamma) \cdot e^{j\psi(\gamma)} \quad ,$$

has been determined, it is assumed that when the whole structure is used as a retrodirective antenna, the ith radiator will retransmit a pattern given by

$$D_i\, B(\gamma + \Delta_i)\, e^{j[\psi(\gamma + \Delta_i) - \psi(\Delta_i)]} \quad ,$$

which gives each of the pseudo-omni patterns a net electrical phase angle equal to zero in direction $\gamma = 0$.

Using the principle of superposition, these N complex patterns are summed to obtain the final retrodirected transmitter pattern. The azimuthal position of the ith elemental radiator is defined by Δ_i, and D_i is an amplitude weighting function. As has already been mentioned, for Mode 1 operation $D_i = 1$, and for Mode 2, $D_i = B(\Delta_i)$.

The conjugate networks assure that in the retrodirection, all the elements add in phase regardless of the complexity of the radiation pattern characteristics in that direction. There is, however, no assurance that any particular element will contribute to the gain in the desired direction, since the elemental pattern may have a null in that direction.

b. Computation of Azimuthal Gain

In order to determine the gain of any given antenna, the peak power of the radiation pattern is compared with the average power radiated in all azimuthal directions. This average power can be computed in several ways, and at least two methods were employed for each of the computed patterns presented in this report. These methods are as follows:

Method 1. Compute the average scalar power value of the pseudo-omni single-element pattern and then add the contribution from each of the N elements, without regard to phase relationship. The average value can only be approximated, since the pseudo-omni pattern, like the final radiation pattern, is only computed every $\frac{360}{M}$ degrees, which in practice is relatively large compared to the ripples in the pattern. This is obvious in the plot of $B(\gamma)$ in Fig. 4, where $M = 180$. Expressed in dB, this average value is given by

$$H = 10 \, \log \frac{1}{M} \left(\sum_{j=1}^{M} B_j^2 \right) \left(\sum_{i=1}^{N} D_i^2 \right) \quad .$$

17

Method 2. Compute the average scalar power value of the final radiation power pattern, $S(\gamma)$. For reasons similar to those given above, this method is only approximate and should give similar accuracy. Again, expressed in dB this average value is given by

$$W = 10 \log \frac{1}{M} \sum_{j=1}^{M} S_j \quad .$$

Method 3. Instead of assuming that each element reradiates the conjugate phase, it is assumed that each radiates with equal phase. (This mode of operation may well be used in practice to establish contact between two adaptive antennas.) The final radiation pattern is then computed in the same way, and should result in an approximately omnidirectional pattern. This pattern will have at least N ripples in it, but its avarage value is readily estimated and is designated by T.

Method 4. Compute the average power value of the radiation pattern within the cylindrical lens and sum the contribution from each element without regard to phase relationship. Expressed in dB, this average value is given by

$$Q = \frac{C}{2\pi} \int_{-\pi}^{\pi} G(\alpha)^2 \, d\alpha \sum_{1}^{N} D_i^2 \quad ,$$

where C is a normalization factor relating power density within the cylindrical lens to power density radiated from the biconical horn.

c. Results of Some Computations

Table I shows the results of some sample computations which are associated with the computed antenna patterns shown in Figs. 6 through 13. Also tabulated are some of the input parameters. It should be noted that the plotting machine is not capable of predicting the peak value of the side lobes.

It has been shown by Cutler et al.[1] that the mamimum overall antenna gain G' of N elements, each with a gain of g', and with the elemental main lobes directed more or less uniformly in all directions, is given by $G' = N/g'$. The same arguments can be used to show

18

Table I

VALUES OF CERTAIN PARAMETERS FOR FIGURES 6-13

Fig. No.	R	L	N	K	Mode	Gain 1	Gain 2	Gain 3	Gain 4	P	Beamwidth
6	10	3	60	0	1	17.13	17.10	17.35	16.99	17.78	4.2°
7	10	3	60	0	2	17.42	17.41	–	17.19	17.78	4.4°
8	10	3	90	0	1	19.09	19.15	–	18.70	19.55	3.4°
9	10	3	90	0	2	19.53	19.47	–	–	19.55	3.2°
10	10	3	30	0	1	13.01	12.99	–	12.91	14.77	5.5°
11	10	3	30	2	1	13.01	12.99	–	12.91	14.77	5.5°
12	5	3	30	2	1	14.27	14.24	14.49	14.11	14.77	8.0°
13	5	3	30	2	2	14.65	14.65	–	–	14.77	8.3°

Note: The header "PARAMETER" spans columns R through Beamwidth.

that the maximum gain for an antenna which only radiates in the azimuthal direction is also given by $G'' = N/g''$, if g'' is now the azimuthal gain of each element. The overall azimuthal gain G'' obviously has a maximum value of N when g'' is unity, that is, when the elemental antennas have omniazimuthal patterns. It is assumed that these elements are randomly located in free space, with their radiation planes all parallel, and that they are sufficiently separated from each other that all mutual coupling effects are negligible. This gain is realizable in any azimuthal direction provided the elements are appropriately phased and power is equally divided among them. Hence, the maximum theoretical gain to be expected from any of the antennas for which patterns were computed, expressed in dB, is

$$P = 10 \log N \quad .$$

This value is also tabulated for comparison in Table I.

FIG. 6 PATTERN FOR 20-WAVELENGTH DIAMETER ANTENNA OF 60 EQUAL-POWER ELEMENTS

20
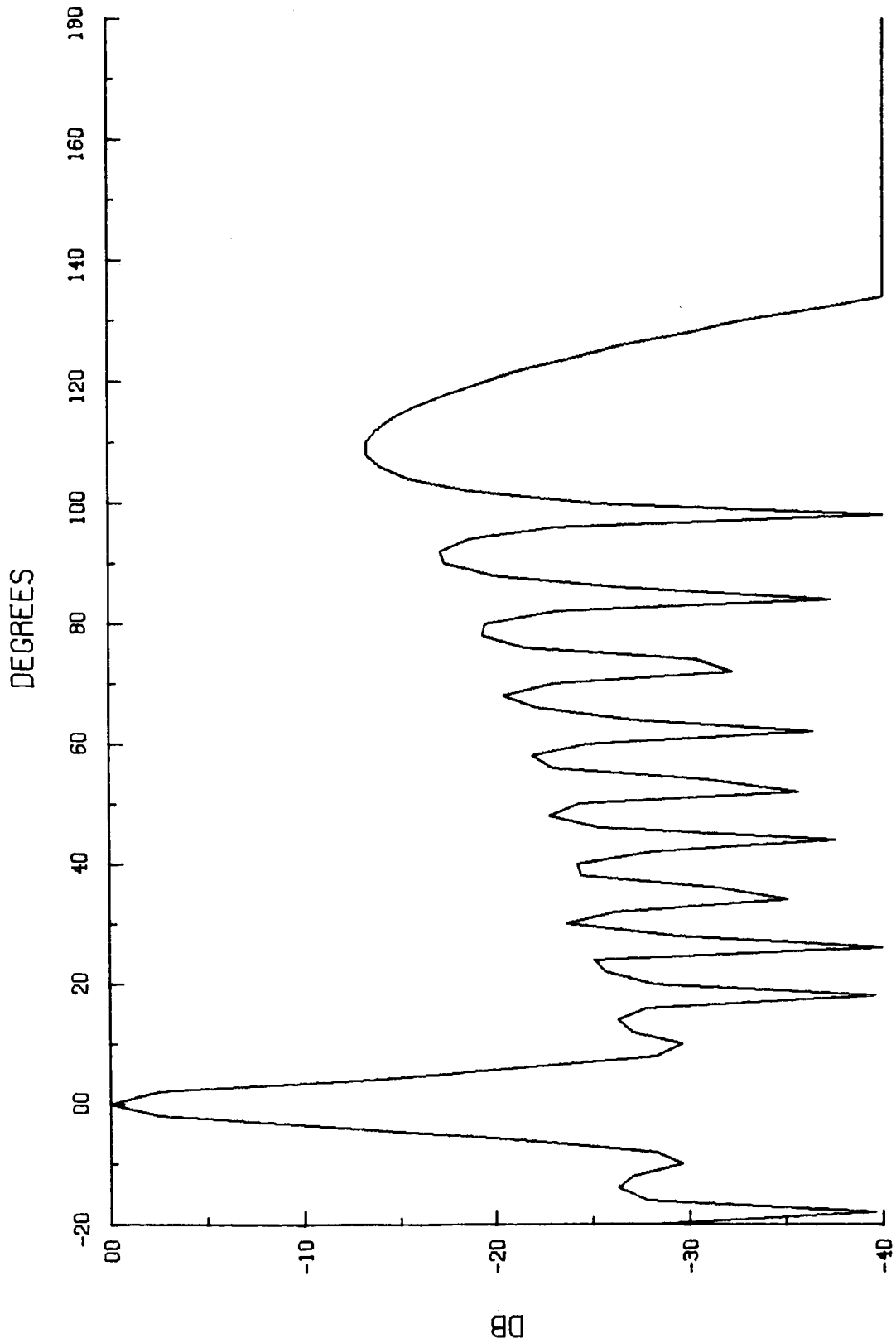
FIG. 7 PATTERN FOR 20-WAVELENGTH DIAMETER ANTENNA OF 60 WEIGHTED ELEMENTS

FIG. 8 PATTERN FOR 20-WAVELENGTH DIAMETER ANTENNA OF 90 EQUAL-POWER ELEMENTS

22

FIG. 9 PATTERN FOR 20-WAVELENGTH DIAMETER ANTENNA OF 90 WEIGHTED ELEMENTS

FIG. 10 PATTERN FOR 20-WAVELENGTH DIAMETER ANTENNA OF 30 EQUAL-POWER ELEMENTS (Symmetrical)

FIG. 11   PATTERN FOR 20-WAVELENGTH DIAMETER ANTENNA OF 30 EQUAL-POWER ELEMENTS (Asymmetrical)
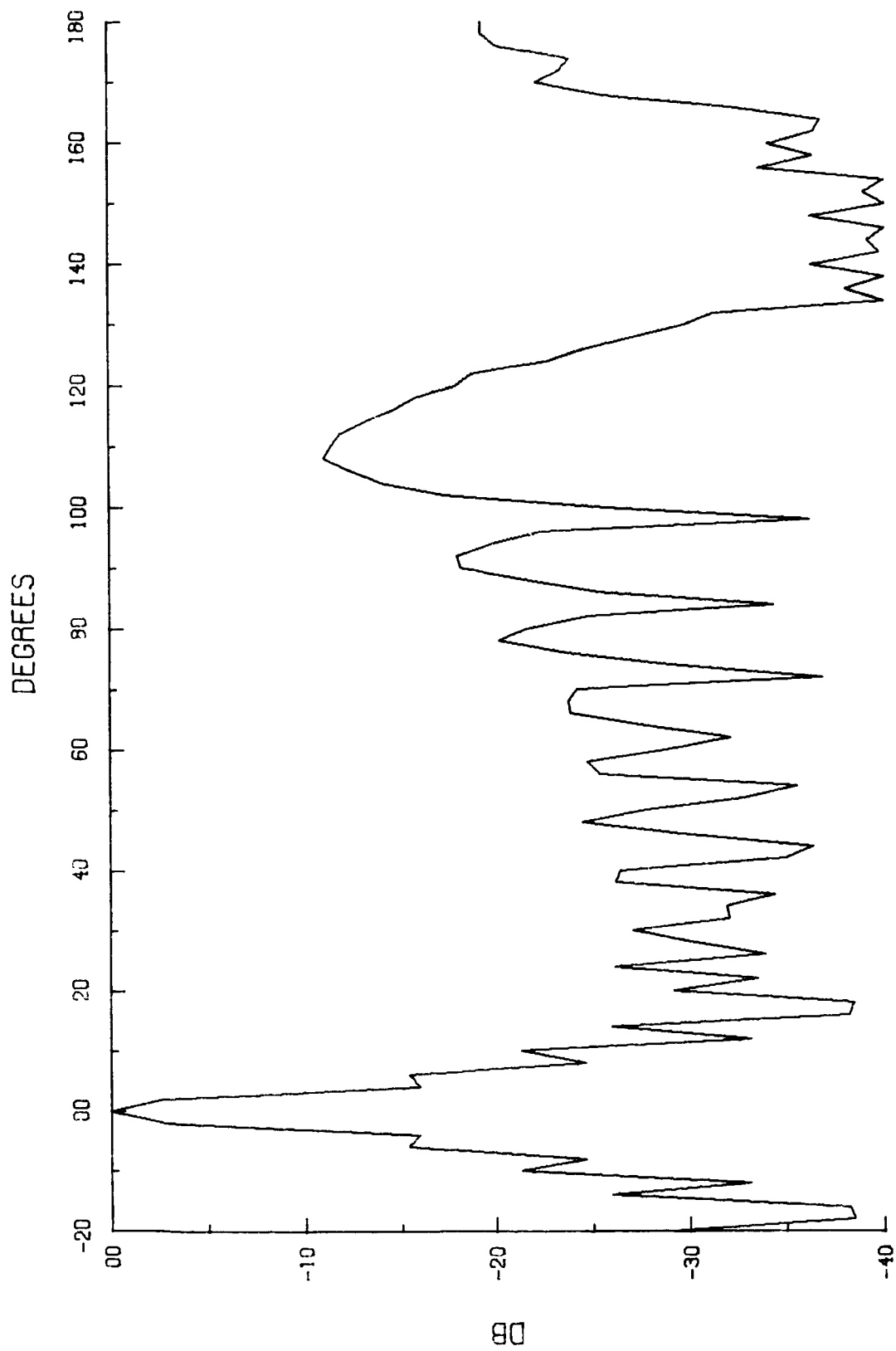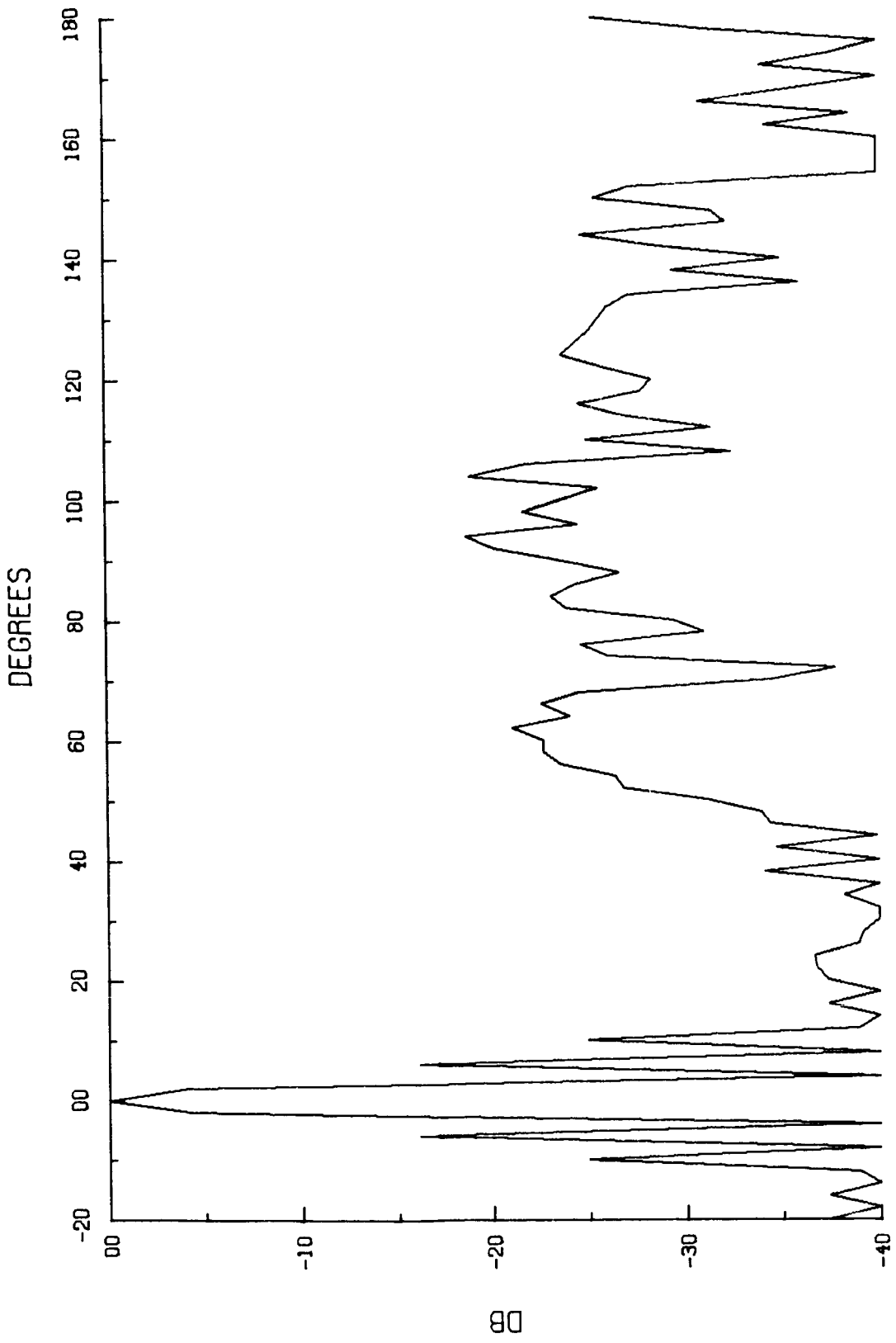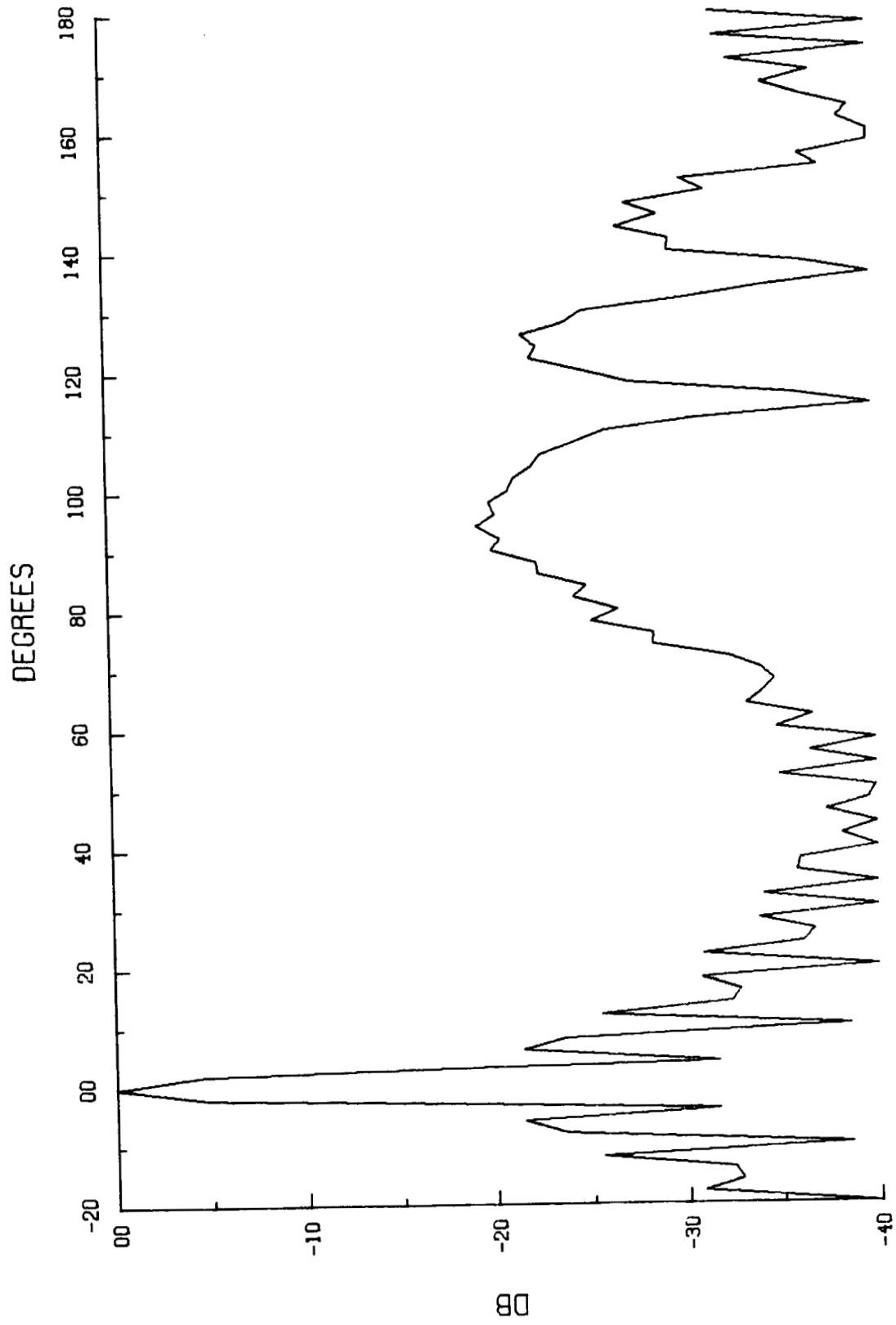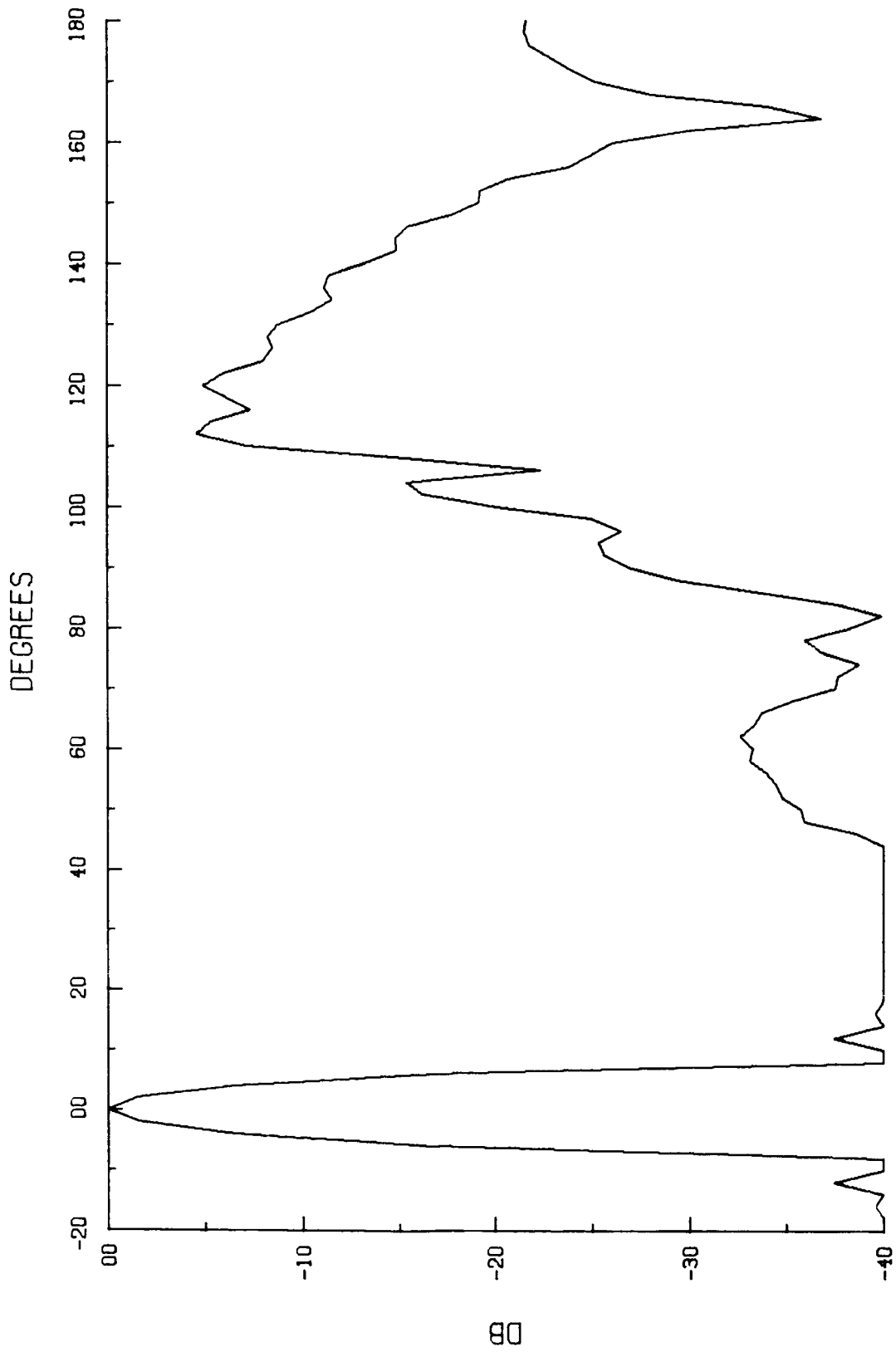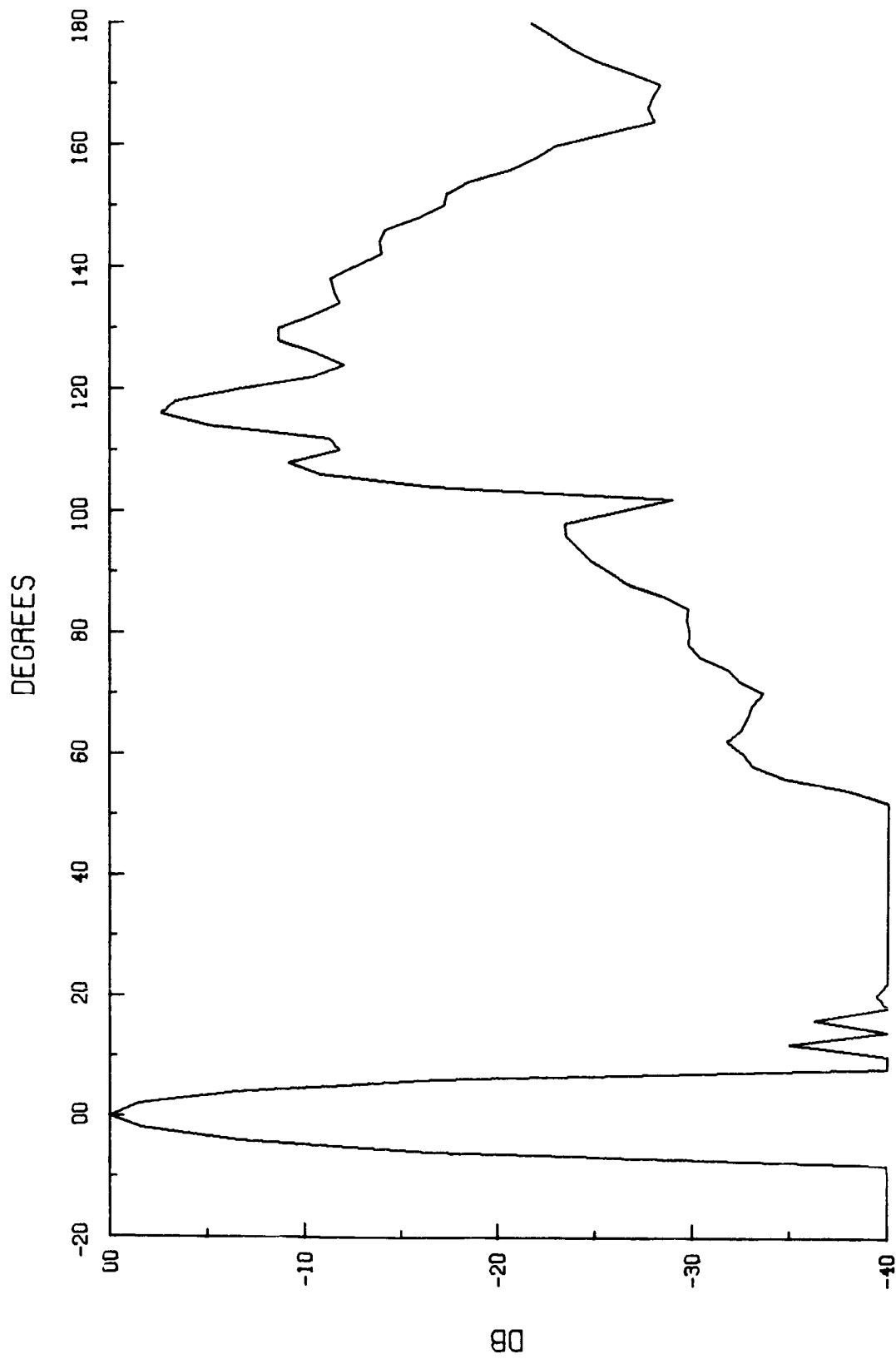
25
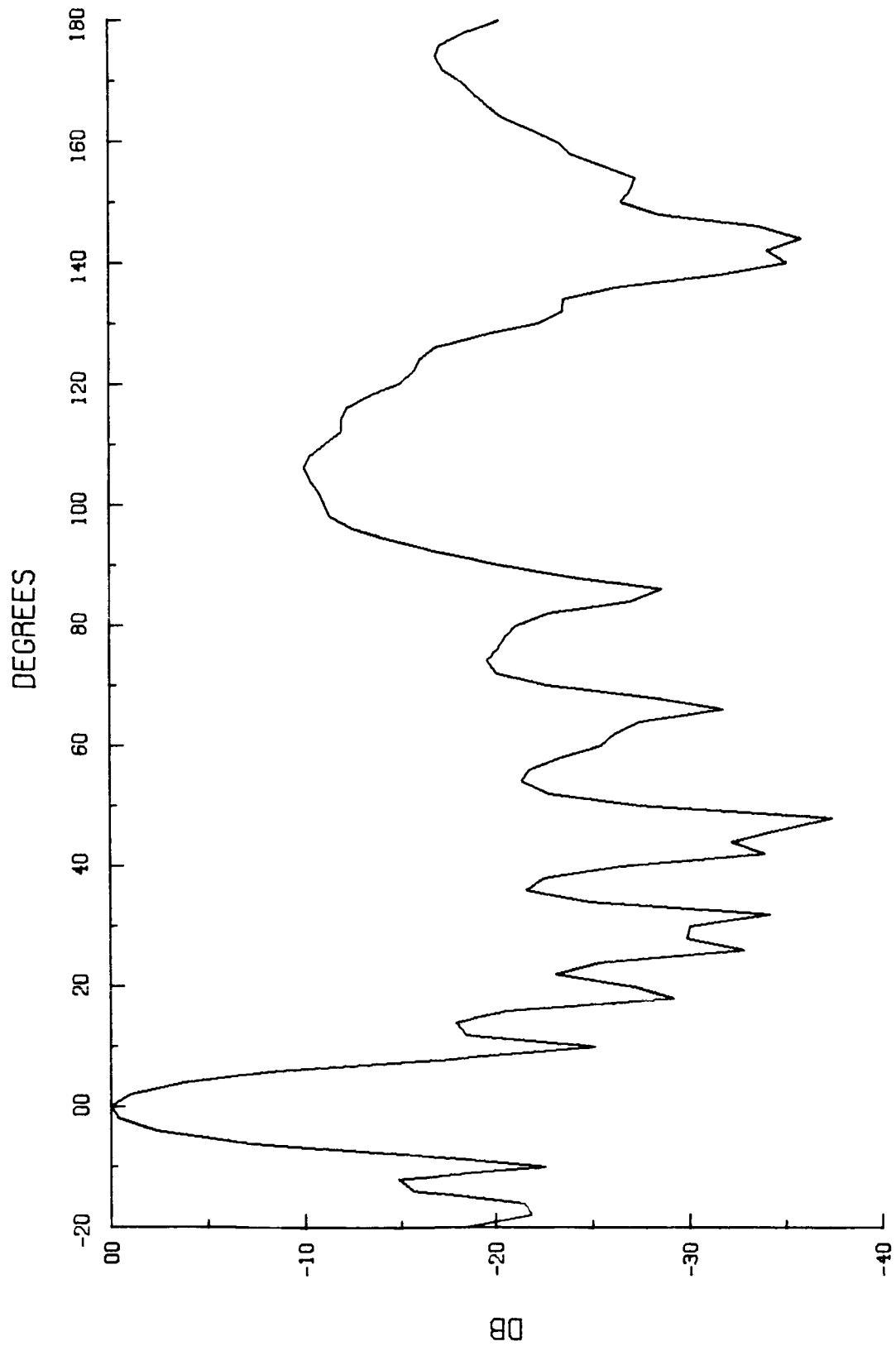
FIG. 12 PATTERN FOR 10-WAVELENGTH DIAMETER ANTENNA OF 30 EQUAL-POWER ELEMENTS
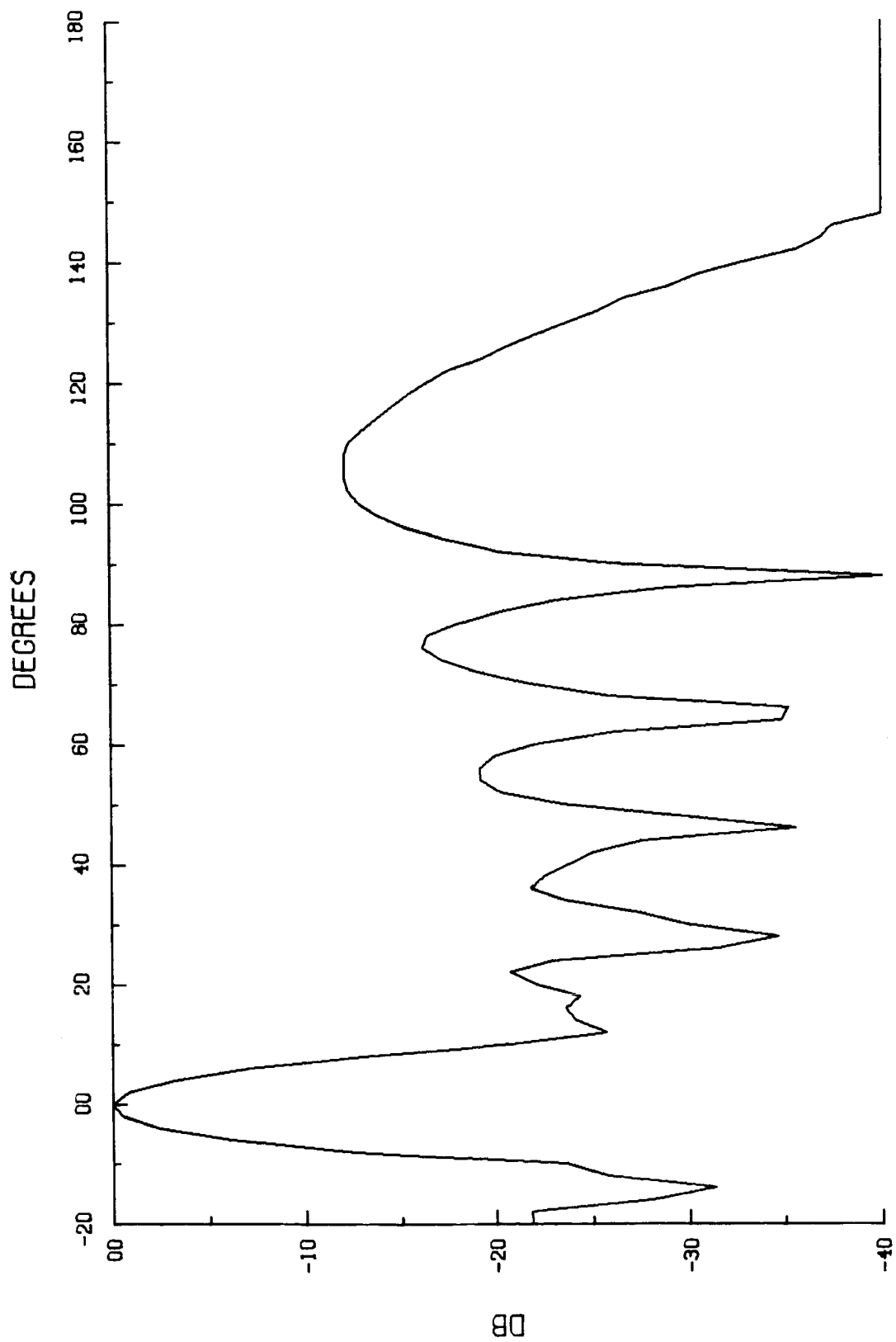
FIG. 13 PATTERN FOR 10-WAVELENGTH DIAMETER ANTENNA OF 30 WEIGHTED ELEMENTS

27

The following is an explanation of the input and output parameters appearing on each of the computed patterns. The quantity V is the computed maximum radiated power density in dB.

R = radius of cylindrical lens, measured in units of λ

L = length of cylindrical lens, measured in units of $R\lambda$

N = number of elemental radiators

K = angle (in degrees) between the retrodirection and the arientation of the closest elemental radiator. The patterns are symmetrical if K = 0 or $\frac{360}{2N}$

Mode 1 assumes saturated amplifiers

Mode 2 assumes linear amplifiers

Gain (1) = the azimuthal gain computed by Method 1 = V − H

Gain (2) = the azimuthal gain computed by Method 2 = V − W

Gain (3) = the azimuthal gain computed by Method 3 = V − T

Gain (4) = the azimuthal gain computed by Method 4 = V − Q

P = postulated "maximum theoretical gain" = 10 log N

Beamwidth = the 3-dB beamwidth, in degrees, estimated from the computed pattern.

Although the computed patterns have not yet been fully analyzed, the following significant points are apparent:

(1) The side-lobe levels are relatively high, and in some cases so high they reduce the maximum gain appreciably.

(2) The postulated maximum theoretical gain is everywhere greater than any of the computed values of gain, out is approached in Mode 2 operation. This somewhat impractical mode appears to provide a few tenths of dB increase in computed gain over an otherwise similar

antenna operating in Mode 1, and it also provides more "well behaved" side lobes, but it is considered to be of only academic interest.

(3) There is an apparent gain increase of 1.2 dB when the antenna diameter is halved but N is kept constant at 30. As can be seen from the curves, the larger antenna has the narrower beamwidth but its lower gain is accounted for by the large side lobes.

(4) If only every alternate element of the 60-element antenna were used to radiate the available RF power, with the unused elements terminated, it is postrulated that there should only be a loss of gain of about 3 dB. Such an antenna would appear to have about 1-dB more gain than the computed case for a similarly sized antenna with 30 elements, where the elemental radiators fill the bottom of the cylindrical lens. This indicates that the highest final gain is obtained with elemental radiators having low gain within the cylindrical lens.

(5) Comparing Figs. 10 and 11, there is no apparent change in gain when the peak of the beam is changed by 2 degrees, even though the pattern shapes change. If this is a general rule it is very important, since it means there will be no amplitude modulation of the radiated signal as the vehicle rotates.

(6) The beamwidth of each antenna is much less than the value $\frac{360}{N}$, which represents the maximum beamwidth obtainable if all the power associated with the maximum postulated gain, N, is

concentrated in the main beam. This indicates
that there is a lot of power in the side lobes.
In a purely retrodirective antenna in free space,
only the maximum ERP in the retrodirection is of
consequence, but if the antenna is also to give
directional information or operate in more than
one direction, side lobes, main beam squint,
and other pattern characteristics could be of
some consequence. In the case of a capsule
approaching the planet, side lobe power re-
flecting off the planet could cause serious
interference with the main transmitted beam.

B.   TASK 2 - ENVIRONMENTAL CONDITIONS

Adaptive antennas for space missions, so far restricted mainly to
those of the retrodirective type, are being considered for a planet-
orbiting or fly-by bus, and for an entry capsule. The study of environ-
mental effects during this first quarter of research has been directed
toward characterizing the electromagnetic environment through which the
retrodirective antennas may operate, and towards evaluating the effects
of the electromagnetic enviromnent upon adaptive antenna operation. A
Mars mission is used for descriptive purposes manely to reflect the un-
knowns which exist in characterizing a planetary environment, but the
study should be applicable to more general environments.

A considerable amount of literature has been acquired to provide a
background and reference for the continuing study. The literature search
in particular has been directed toward Mars mission studies and environ-
mental characteristics, and toward environment measurements by electro-
magnetic techniques.

1.   Orbiting or Fly-By Bus

a.   Background

The Mars bus, in the orbiting or fly-by mode, will be
in the Martian ionosphere or in the near interplanetary space. The

entry and lower atmospheric environment is discussed for an entry capsule.

The transmission environment for the bus and bus-earth link includes the planet atmosphere, interplanetary space, and the earth's atmosphere. Also, signals will be reflected from the planet. These planetary reflections can modify retrodirective operation by inducing noncancelling phase errors between array elements and by inducing amplitude interference both at the array elements and at the receiving terminals of the retrodirective link. The extent of modification is being investigated. Other effects of the transmission environment do not appear to differ for retrodirective antenna operation or any other antenna operation.

A very important consideration for retrodirective links is the modification of the electromagnetic signatures of the transmission environment (i.e., amplitude, phase, and frequency). The electromagnetic signatures are important because they affect signal acquisition, vehicle tracking, effective transmitted signal strength, and scientific exploration.

Recent studies by SRI and others[2,3,4] indicate that a limitation to the reception of deep space signals on the earth is the random fluctuation in refractivity of the transmission media. Time fluctuations in refractivity cause phase jitter, which reduces the gain of large antennas and the signal phase coherence in antenna arrays of large aperture. Phase jitter also presents a pointing problem for large antennas with narrow beamwidths.

Phase jitter in the transmission medium near the bus will cancel along the return signal path, because the conjugate of the phase jitter (the phase jitter along the pilot signal path) will be radiated by the subapertures of the retrodirective array. The spatial characteristic scales of significant phase near the bus are expected to be large compared to the size of a subaperture,* and the associated time-varying

---

*If the subaperture size is larger than the characteristic scales of phase jitter, the associated signal phase summed over the subaperture would be random, and cancellation could not occur. This, however, is not a practical situation for a retrodirective array on a Mars bus.

refractive medium should be time coherent during the signal transit. Far away from the bus, the associated time-varying refractive medium may change during signal transit time, and the phase jitter may not cancle (for example, phase jitter induced by the earth's atmosphere). This does not affect coherent signal formation since characteristic scales of phase jitter will exceed the size of the retrodirective array, and rays from subapertures will essentially lie along the same transmission path.

Gross refractive characteristics of the transmission environment are important in determining the position and velocity of spacecraft and in determining the apparent angle to receive a space-probe signal (particularly during the ground station acquisition phase). Refraction will cause the bending of the transmission path from the geometrical direction and the lengthening of the transmission path in excess of the geometrical path length. Retrodirective array operation does not eliminate gross refractive bending (the transmission paths of the pilot and return signals is unchanged).

b. Earth's Atmosphere

The transmission environment of the earth's atmosphere is substantially documented in the literature[2,3,4] and will not be reviewed here. It is important to note that the correlation times of the random fluctuations in the earth's refractive media (troposphere and ionosphere) are less than the signal transit time between Earth and Mars (300 to 1300 sec). Thus, phase jitter induced by the earth's transmission environment will not be equal for the pilot signal path and the return signal path. The gross refractive signature of the earth's transmission environment may also not be equal on the pilot and return paths. The earth terminal antennas will be pointed in different parts of the earth's atmosphere for transmission and for reception (for example, a difference in earth elevation angle of 5 degrees), and the pilot and return paths may not be equal in length.

It is thus concluded that retrodirective cancellation of phase delays along pilot and return paths will not be complete for deep

space to earth applications. Conceivably, the phase delay signature could be eliminated for near space and for capsule-to-bus applications.

c. Interplanetary Space

Typical plasma characteristics of the interplanetary space are summarized in Table II. The solar interplanetary plasma is

Table II

TYPICAL PLASMA CHARACTERISTICS OF

INTERPLANETARY SPACE[4]

Solar Interplanetary Magnetic Field

Strength - At 1 A.U., average 2 or 3 gammas 0 to 100 gammas

Between 1 A.U. and 1.75 A.U., average $<$3 gammas (lack of definite data exists at these solar distances).

Strength depends upon solar activity. Fluctuations of one or two orders of magnitude occur, depending upon solar activity.

Solar-Wind Electron Streams

Solar Condition	Minimum		Maximum	
	Gas Flow	Electron Density	Gas Flow	Electron Density
Quiet sun	600 km/sec	5 elec/cm^3	25,500 km/sec	0.12 elec/cm^3
Disturbed sun	1500 km/sec	100 elec/cm^3	63,000 km/sec	2.3 elec/cm^3

Minimum Scale of Electromagnetic Irregularities

Gyro radius of electrons $\gtrsim$ 10 meters

Gyro radius of ions $\gtrsim$ 1 km

Mean Free Path of Electrons and Ions

$\gtrsim 10^5$ km

seen to be weak relative to the magnetic field and electron density in the earth's ionosphere. The gyromagnetic frequency in the earth's atmosphere is 1.42 Mc, which is large compared to the gyromagnetic frequency in interplanetary space, typically 0 to 300 cps. The maximum

plasma frequency in the earth's ionosphere is typically 2 to 20 Mc, which is also large compared to the plasma frequency in interplanetary space, typically 0 to 90 kc.

The long transmission paths into deep space have caused concern about the integrated effects of refraction, RF attenuation, and Faraday rotation in the interplanetary medium, even though the unit plasma in it is weak. Considerable data concerning the gross transmission characteristics of the interplanetary medium are available. Summarizing from Ref. 6, the evaluation of gross characteristics are:

Refraction--The transmission path length at S-band varies relative to the geometrical path length by less than 1 part in 10^{13}/sec; the difference between the transmission and geometrical path lengths is less than 2 parts in 10^6 at large ranges.

RF Attenuation--The RF attenuation of S-band signals is less than a total of 1 dB at distances as high as 200×10^6.

Faraday Rotation--The amount of power coupled from one mode of polarization to the other mode of polarization on a round-trip Venus-Earth path is less than 31dB at S-band; thus, rotation of the plane of polarization is less than 0.1 percent.

The above data represents a considerable spatial and temporal coverage of interplanetary space and should be representable as typical results. Unfortunately, no correlation has been made with solar activity. The effects could conceivably be larger for extreme solar activity.

The difference between transmission and geometrical path lengths is much larger for the interplanetary medium (kilometers) than for the earth's ionosphere (ten to hundreds of meters). From an engineering point of view, refraction does not limit ground-based radio guidance of spacefraft.[*]

---

[*]The ground-based radio guidance of spacecraft is accomplished by obtaining range and velocity data from doppler signatures in the telemetry signal. The angle data is obtained from antenna pointing data and from the cumulative matching of the range and velocity data with theoretical trajectories.

The effects of random fluctuations in the refractive index of the interplanetary medium are difficult to assess. Normally, the effects of fluctuations in the interplanetary medium should be hidden by the effects of fluctuations in the earth's ionosphere. Only under disturbed conditions and when continuous blob structure exists through Earth planet space will the fluctuations in the interplanetary medium be comparable to fluctuations in the normal ionosphere. It is conceivable that the effects of random fluctuations (and other anomolies) in the interplanetary medium are so rare in occurrences and severity that the effects are inseparable from ionospheric effects measured by sensors on the earth's surface. The interplanetary medium is being studied through experiments on Pioneer spacecraft.

d. Mars' Atmosphere

The transmission environment in the atmosphere of Mars has not been experimentally defined. Final results of the recent Mariner radio occultation experiment[7],[8] have not yet been published. The radio occulation experiment was concerned with the measurement of refractive effects in the electromagnetic signatures of the bus-to-earch signal at occultation. Refractive effects in the amplitude, phase, and doppler signatures of the received signal were to be used to deduce surface pressure and scale height in the lower atmosphere and to deduce ionization and scale height in the Martian ionosphere. Unconfirmed reports concerning the experiment have not indicated gross effects in excess of what would be expected from an earth model. A cool ionosphere with an electron density about 0.1 that of the earth has been indicated. The lower atmosphere is believed to be composed almost entirely of carbon dioxide, and a surface pressure of 6 mb is now postulated.

There is speculation that recent estimates of low surface pressure and that larger amounts of CO_2 and less amounts of N_2 than expected could cause a larger electron density in the Martian ionosphere than the 10^5 elec/cm^3 postulated from an atmospheric model with a surface pressure of 85-mb and a composition containing 83-mb N_2 and 2-mb CO_2.[9],[10] Thus, refractive effects due to the ionosphere could mask the

refractive effects of the lower atmosphere and cause erroneous prediction
of surface pressure and scale height in the lower atmosphere. Results
of the radio-occulation experiments do not provide exact surface pressure,
because no absolute altitude scale is available.

The effects of retrodirective antenna operation on a
similar Mars occulation experiment should be reviewed.

Magnetometer and trapped-radiation measurements of the
Mariner fly-by have indicated that no magnetic field exists near Mars
in excess of the ambient magnetic field of interplanetary space. Thus,
the transmission environment in the Martian ionosphere should be reci-
procal. The effects of Faraday rotation, of anisotropy due to field-
aligned ionization, and of other phenomena induced by the magnetic field
and magnetic disturbances observed in earth's ionosphere will not occur
in the Martian ionosphere (or in interplanetary space).

It is expected that electromagnetic signatures of the
Martian atmosphere will be obtained from the capsule-to-bus telemetry
signal. Interpretation of the signature, however, may be complicated
by uncertainties in the entry environment. Practical retrodirective
arrays would require frequencies at which the wavelength is much less
than the vehicle dimensions. Such frequencies ($\gtrsim$ 100 Mc) would com-
promise measurements of Martian ionosphere, since ionospheric effects
at these frequencies would be practically negligible.

2. Entry Capsule

a. Background

During atmospheric braking entry a plasma sheath is
formed around the vehicle. A wake or trail is also formed in the rear-
ward void of the vehicle. Ionization in the sheath around the vehicle
arises from three sources: thermal ionization caused by the compressive
shock wave, thermal ionization generated by viscous effects in the boun-
dary layer, and chemical ionization produced as ablative heat-shield
material is introduced into the boundary layer. During entry the wake
behind the vehicle transforms from laminar flow to turbulent flow and

the ionization characteristics become turbulent. If propulsive slowing down of the bus is employed, ionization is also created by rocket exhausts.

Usually electron density in the sheath around an entry vehicle is predicted by thermal ionization caused by the compressive shock waves. The characteristics of the compressive shock wave are determined by the gas composition of the atmosphere, by the structure of the atmosphere, by the entry flight profile, and by the physical parameters of the entry vehicle.

b. Martian Atmosphere Models

Defining the gas composition of the Martian atmosphere from Earth-based astronomy is limited by atmospheric attenuation and the radiating bands of possible species. Only carbon dioxide (CO_2) and water vapor (H_2O) have been positively identified. Nitrogen (N_2) and argon (A) have been proposed as other constituents of the atmosphere. The gas compositions of various models of the Martian atmosphere are given in Table III, below.

Table III

VOLUMETRIC COMPOSITION OF MARTIAN ATMOSPHERE

	Kaplan[11]					Spiegel[12]		deVaucouleurs[13]
	10 mb* (percent)	25 mb* (percent)		40 mb* (percent)		41 mb* (percent)	133 mb* (percent)	85 mb* (percent)
CO_2	60	16	16	8	7	0.7	7.2	0.3
N_2	20	76	8	45	88	98.7	86.8	98.5
A	20	8	76	47	5	0.6	6.0	1.2

*surface pressure

The dense atmospheres, 41 to 133 mb, are based on optical measurements,[12,13] assuming a purely Rayleigh scattering atmosphere, and are believed to be upper bounds. The thinner atmospheres, 10 to 40 mb, are based spectroscopic observation of the CO_2 content in the

Mars atmosphere.[10]   (Unfortunately, these models are based on analysis
of a single photographic plate, thus reducing the reliability of the
results.)   Unconfirmed reports of the Mars occultation experiment point
to a 6- to 10-mb surface pressure, the lower value being favored.

The atmospheric structure as a function of altitude above
Mars is either postulated on theoretical considerations or is simulated
from the earth's structure.[14,15]   This uncertainty in altitude structure,
in addition to uncertainties in surface conditions, compound the un-
certainty in man's knowledge of the Martian atmosphere.   For example,
the decrease of gas density from the surface to an altitude of 120 km
may be two orders of magnitude for one model and six orders of magnitude
for another model.[16,17]

Models of the Martian atmosphere are certainly not con-
clusive, and the concurring problems in mission design are frequently
discussed in the literature.   NASA engineering models[14] tend to be based
on surface pressure observations of Kaplan (P = 25 ± 15 mb as compared
to 1031 at the earth's surface) and on altitude structure presented by
Levin.

c.   Electromagnetic Blackout

A measure of the existence of electromagnetic blackout,
which occurs when the critical plasma frequency exceeds the signal fre-
quency, is usually predicted using normal shock parameters and equili-
brium electron densities for the various postulated atmospheric models.
The plasma frequency has been predicted as a function of altitude and
shock speed.   This approximation of blackout applies to blunt bodies
in the stagnation region.   However, plasma density around a body gener-
ally decreases rapidly when plasma conditions in the stagnation region
decrease rapidly.   Thus, a measure of plasma frequency along the direc-
tion of capsule motion can indicate frequency-sensitive effects on
propagation and bus-to-capsule communication in other directions.   Usu-
ally an order of magnitude or loss decrease in plasma frequency is
assumed for transmission at the side or back of the capsule.

Effects of entry plasma on communications are not easily predictable. Idealized propagation concepts, such as plane-wave propagation, can be completely inadequate to describe propagation in entry plasma. The critical plasma frequency, a measure of blackout effect, is usually based on reflection for plane-wave propagation. Signal degradations can be large when electron densities are lower than the critical for the frequency used.

Equilibrium electron density for Kaplan and Speigel models of the Martian gas compositions are available from the literature. Blackout parameters for Spiegel models have been plotted using appropriate shock parameters.[18] Considering, for instance, the 100-Mc transmission frequency by Beuf,[19] blackout occurs in the 41-mb Speigel model for velocities greater than 20,000 ft/sec at 160,000 feet, and greater than 15,000 ft/sec at 100,000 feet. Blackout conditions for this model do not appear to exist for speeds less than 10,000 ft/sec at any altitude. However, for the denser 133-mb Spiegel model, speeds less than $\approx$ 7000 to 8000 ft/sec are necessary if frequencies of 100 Mc are not to be severely attenuated during entry.

Unfortunately, shock parameters for the Kaplan models of the Martian atmosphere have not been found in the literature search. However, in Ref. 20 blackout has been studied using an 11-mb atmospheric model and a composition of 40-percent N_2, 30-percent CO_2, and 30-percent A. This model is roughly equal to the low-pressure Kaplan model. In Ref. 20, blackout was considered for atmospheric braking at entry angles of 20 and 90 degrees. An entry velocity of 26,600 ft/sec at 656,000 feet and a ballistic parameter of 0.2 slugs/ft^2 were assumed. Electron densities as high as 10^{15} elec/cm^3 in and near the stagnation region were predicted. A two-order-of-magnitude decrease in density in the wake was predicted, assuming frozen isotropic expansion. Blackout extinguishes sharply at an altitude of 60,000 feet for the 90 degree entry angle, and extends below 60,000 feet for the 20 degree entry angle. Blackout in the stagnation region is shown to begin at 530,000 feet for both entry angles, assuming an RF frequency of 2300 Mc. For a 100-Mc

signal, blackout is shown to begin at the entry altitude of 656,000 feet. Ionization by ablation products could extend blackout to lower altitudes.

d. Uncertainties

If the surface pressure is 6 mb (and there is increasing evidence for it), the blackout predicted in Ref. 20 would extend practically to the surface. Thus, propulsive braking may be required to slow the entry capsule down and to eliminate blackout. Propulsive braking, however, creates ionization through rocket exhausts, and transmission through the rocket exhaust environment must be considered. An alternative to propulsive braking is to modify the plasma, for instance by the injection of a high-electron affinity fluid into the sheath. Such a fluid, carbon tetrochloride, has been proposed for reducing the electron density in the wake of an entry vehicle.[20,22]

It is apparent that blackout predictions are very uncertain, because little is known about the atmospheric constituents and the recombination rates of electrons in the flow processes. Uncertainties about the ionization effects of ablative material also exist, and plasma modification and propulsive braking compound these uncertainties. The uncertainties in the entry environment limit electromagnetic techniques to measuring altitude (radio altimater and radio ranging) and velocity (doppler). The interpretation of environmental characteristics from electromagnetic signatures is also limited.

Even when the ionization around the capsule falls below the blackout level, viscous effects in the boundary layer and turbulence in the wake must be considered in regard to multipath fluctuations in amplitude and phase. Characteristic scales of turbulence near the retrodirective antenna may be smaller than the size of subapertures in the array. Thus, the associated phase jitter summed over the subaperture may be random, and retrodirective phase cancellation may not occur. Multipath amplitude fading may also exist for transmission through the viscous and turbulent entry plasma. The phase and amplitude fluctuations would be similar to the fluctuations in HF and VHF signals propagation through the earth's ionosphere. The fluctuations, however,

should have a higher frequency than the vehicle doppler shift. Thus, the fluctuations may interfere with doppler measurements. Fluctuation effects would be difficult to evaluate theoretically, and an experimental investigation would be required.

The modification of antenna patterns and impedance during entry and the radio noise generated by thermal effects subsequent to blackout are important considerations for an entry communication system. These parameters, not easily calculated, can be studied in the laboratory using simulation techniques. Differences between theory and experiment can be considerable. During entry, the antenna near fields alter the antenna impedance and far-field radiation characteristics by (1) dissipating energy normally stored in near fields and (2) redistributing near fields and surface currents, in addition to the usual wave attenuation. Decreases in far-field radiation exceeding 10 dB have been measured. These decreases are caused by the near-field effects alone at plasma frequencies less than critical.[23],[24]

Adaptive antenna operation and retrodirective antenna gain will have to be measured in simulated plasmas to prove the adaptability of the adaptive concept to entry capsules. The effects of ablation are important relative to destructive effects on the retrodirective antenna as well as increasing ionization in the plasma.

In evaluating the operation of a retrodirective antenna on an entry capsule, planetary reflections will be of considerable significance.

III ANALYSIS

A. THE CYLINDRICAL GEODESIC LENS ANTENNA

The results so far obtained from this antenna appear very encouraging. The particular antenna configuration for which results so far have been computed, namely the biconical horn antenna, does not at present appear to be a practical device for achieving maximum ERP, particularly if only a narrow axial plane beamwidth is necessary. Results so far obtained indicate that the maximum ERP is proportional to the axial plane gain multiplied by the number of elemental transmitters. However, a high axial plane gain, i.e., a narrow vertical beamwidth, can only be tolerated when the desired direction of transmission can be defined within comparably narrow limits. This implies that the desired spin-axis orientation must be well maintained, and if the same adaptive antenna is to be used on the bus for communication to both the earth and the capsule, that all the orbital paths must be essentially in the same plane.

It is possible to stack two or more antennas of the type so far discussed in order to control beam pointing in the vertical or axial plane as well as in the azimuthal plane. However, there does not appear to be any great advantage to this, since the ERP would still be proportional to the axial gain of one of the stacked antennas (all of which are assumed to be equal) multiplied by the total number of elemental transmitters. Thus, axial stacking of antennas will probably not be considered any further.

If the direction of transmission or reception of the adaptive antenna does not lie close to the plane perpendicular to the axis of spin, the biconical antenna could be quite satisfactory. However, for the present it is being assumed that a somewhat higher gain, or narrow axial plane beamwidth, is desired, and this is why work is progressing on analysis of the different type of antenna shown in Fig. 2. The general results are expected to be somewhat similar to those shown in Table I for the biconical antenna; however, greater care with assumptions is

considered necessary with the discrete line-source radiator antenna, therefore many more computations are required before a single antenna pattern is achieved.

The results shown in Table I, where the antenna gain is computed by several different methods, does indicate a satisfactory degree of consistency and gives confidence in the rise of similar techniques for analysis of other antenna configurations. Aspects which have not yet been investigated are the effects of satellite spin rate and RF bandwidths; these are evidently of some consequence because of the rapid changes in amplitude and phase expected within any antenna of the general type now being considered. Reference to Fig. 4 shows how rapidly these functions vary as a function of azimuthal angle γ.

The computer programs have been expressly designed for the investigation of the effects of frequency change, or bandwidth, because R, which is proportional to frequency, is the only basic parameter which is dependent on frequency. The ripples which appear in the so-called pseudo-omni pattern will tend to limit the effective operating bandwidths of the antenna, and when combined with spin of the antenna will impose limitations on the operation of any phase-lock loops which may be employed in the adaptive circuitry. This is particularly true if the antenna is used as a self-adaptive receiving antenna.

One of the significant points to emerge from the study so far is that the maximum ERP of any antenna which can be phased to direct its beam in any azimuthal direction is obtained when omniazimuthal elements are used, provided the elements do not have any mutual coupling or blocking effects. This is theoretically possible if the elements are well separated from each other. Such separation is not always possible or practical, and a start is being made on the investigation of somewhat more practical (and therefore mutually coupled) arrays of omniazimuthal elements.

B. THE ENVIRONMENTAL EFFECTS

Much of the analysis of this problem has been included in Sec. II of this report. The following is a summary of the significant points.

43

It is apparent that environmental constraints on retrodirective array operation are more serious for the entry capsule than for the orbiting or fly-by bus. Electromagnetic signatures (amplitude, phase, and frequency) for the earth-bus link are readily calculated within reasonable limits. The effects of planetary reflections are an important consideration for the earth-bus link and require investigation. Descriptions of the electromagnetic signatures for the capsule-bus link are not easily defined, owing to uncertainties in the atmospheric structure and composition, uncertainties in the characteristics of the entry plasma surrounding the capsule, and the planetary reflections. A plane-wave model does not exist in the entry plasmas, thus evaluation of retrodirective antenna operation of the entry capsule will require measurement in simulated environments. Unsolved problems of thermal ionization by ablation, of plasma modification by chemical ejectants, and of ionization by rocket exhausts complicate any characteristics of the entry environment.

C. SYSTEM ASPECTS

No serious study has yet been given to the system aspects of an interplanetary mission using self-adaptive antennas, but a start will be made shortly. One of the first problems is to determine what frequency should be used between the bus and capsule, and there are some good reasons for using a frequency close to the S-band link from earth to the bus. In this way it is hoped to use the same bus antenna for communicating with both the capsule and earth. Use of such a high frequency would imply that the capsule should also have an adaptive antenna.

Because range and range rate have proved to be such powerful tools for solving many measurement problems, particularly deep space probes, great care will be taken to ensure that the accuracy of these measurements is not lost. It should be noted that to a first approximation there is no doppler shift apparent from a moving retro-reflective array antenna which uses conjugate networks that operate from a self-stabilized local oscillator having a frequency of twice the received (and therefore the transmitted) frequency. One method of retaining the doppler information

44

is therefore to stabilize the local oscillator by means of the incoming signal, which is already shifted by the one-way doppler frequency.

The computational investigations made so far have been concerned with an antenna used in the retrodirective mode, but in the future consideration will be given to the analysis of similar antennas when used as self-adaptive receiving antennas. Such antennas should also be able to give information about the direction of arrival of incoming signals. Although it is not expected to be nearly as accurate as data obtained from range-rate information, this information can be used as navigational information and also, perhaps, for controlling logic to switch out those antenna elements that are not contributing significantly to the main beam. This is another way of making an antenna which can point its main beam in any azimuthal direction while maintaining DC to RF conversion efficiency. Such an arrangement does, however, require total amplifier capacity two or three times as great as the power being radiated at any instant.

IV PROGRAM FOR NEXT QUARTER

Analysis of a more practical adaptive antenna for a spin-stabilized vehicle will be made. Some of the simplifying assumptions previously made will be eliminated; in addition, the effects of bandwidth, doppler shift, catastrophic failure of individual elements, etc., will be investigated.

Investigation will begin on the use of adaptive antennas as self-phasing receivers and for combining the operations of self-phasing, retrodirective radiation, and even simultanious radiation in more than one direction. This will require the consideration of specific circuit components (in block diagram form).

A start will also be made on analysis of the techniques and expected accuracies of an adaptive antenna used as a direction-finding device.

The first quarter evaluation of environmental effects will be applied to the operation of retrodirective array techniques. Particular attention will be given to the effects on the amplitude and phase of planetary reflections. Modifications of electromagnetic signatures (amplitude, phase, and frequency) will also be considered in regard to doppler measurements and environment measurements by electromagnetic techniques.

REFERENCES

1. C. C. Cutler, R. Kompfner, and L. C. Tillotson, "A Self Steering Array Repeater," B. S. T. J., Vol. 42, No. 5, pp. 2013-2032 (September 1963).

2. R. B. Battelle, Ed., "Feasibility Analysis of a Deep-Space Receiving Terminal Array of Large Equivalent Aperture," Final Report, Contract NAS 1-3075, Stanford Research Institute, Menlo Park, California (May 1964).

3. "Investigation and Study of a Multi-Aperture Antenna System," Final Report, Contract NAS 5-3472, Electronic Communications, Inc., Timonium, Maryland (April 1964).

4. P. G. Smith, et al., "Analytical Study to Define an Experimental Program for the Evaluation and Optimization of Multi-Element Large Aperture Arrays," Final Report, Contract NAS 1-3780, Research Triangle Institute, Durham, North Carolina (October 1964).

5. B. B. Lusignon, "Detection of Solar Particle Streams by High Frequency Radio Waves," Journal of Geophysical Research, Vol. 68, No. 20, pp. 5617-5632 (October 15, 1963).

6. M. Easterling and R. Goldstein, "The Effect of the Interplanetary Medium on S-band Tele-Communications," Tech. Report No. 32-825, Jet Propulsion Laboratory, Pasadena, California.

7. G. Fieldbo and V. R. Eshleman, "The Bistatic Radar-Occulation Method for the Study of Planetary Atmospheres," J. Geophysical Res., Vol. 70, No. 1, pp. 3217-3225 (July 1965).

8. A. J. Kliore, et al., "The Mariner 4 Occulation Experiment," Astronautics and Aeronautics, pp. 72-80 (July 1965).

9. R. B. Norton, "A Theoretical Study of the Martian and Cytherian Ionospheres," NASA TN D-2333 (July 1964).

10. V. R. Eshelman, "Radar Astronomy of Solar Plasmas," Scientific Report 4, NASA Research Grant NsG-377, Radioscience Laboratory, Stanford University, Stanford, California (August 1964).

11. L. D. Kaplan, G. Munch, and H. Spinrad, "An Analysis of the Spectrum of Mars," Astrophys. J., Vol. 139, No. 1 (January 1964).

12. G. V. Spiegel, "Effects of Mars Atmospheric Uncertainties on Entry Vehicle Design," Aerospace Eng., Vol. 21, pp. 62-63 and 103-107 (December 1962).

13. G. deVaucoulers, Physics of the Planet Mars (Faber & Faber, Ltd., London, 1953).

14. G. F. Schilling, "Limiting Model Atmospheres for Mars," R-402 JPL, The RAND Corporation (August 1962).

15. G. M. Levin, et al., "NASA Engineering Models of the Mars Atmosphere for Entry Vehicle Design," NASA TND-2525 (1964).

16. G. M. Levin, "A Proposed Solution to Entry Vehicle Design Penalties Caused by Lack of Knowledge of the Mars Atmosphere," AIAA Paper 65-493 (1965).

17. E. D. Shane, "Equilibrium Electron Density on Mars," AIAA J., Vol. 2, No. 8, pp. 1497-1499 (August 1964).

18. F. Bosworth, C. Cook, L. Gilbert, and S. Scala, "Normal Shock Parameters for the Martian Atmosphere," R-63SD12, General Electric Space Science Laboratory (January 1963).

19. F. G. Beuf, "Martian Entry Capsule," Astronautics and Aeronautics, Vol. 2, No. 12, pp. 30-37 (December 1964).

20. D. F. Spencer, "An Evaluation of the Communication Blackout Problem for a Blunt Mars-Entry Capsule and a Potential Method for the Elimination of Blackout," Technical Report 32-594, Jet Propulsion Laboratory (April 15, 1964).

21. P. W. Huber and T. E. Sims, "The Entry-Communications Problem," Astronautics and Aeronautics, Vol. 2, No. 10, pp. 30-40, (October 1964).

22. A. J. Kelly, "An Experimental Feasibility Study of Injectant Materials to Aleinate Mars Entry Communications Blackout," Paper presented at the Third Symposium on the Plasma Sheath, Boston, Massachusetts, September 21-23, 1965.

23. J. B. Chown, et al., "Effects on Re-Entry and Space Environments on Antenna Performance," Paper presented at the Third Symposium on the Plasma Sheath, Boston, Massachusetts, September 21-23, 1965.

24. W. C. Taylor and D. E. Weissman, "The Effects of a Plasma in the Near-Zone Field of an Antenna," Final Report, Contract NASA-3099, Stanford Research Institute, Menlo Park, California (June 1964).